LEARNING EXPLICIT SINGLE-CELL DYNAMICS USING ODE REPRESENTATIONS

Anonymous authors
Paper under double-blind review

ABSTRACT

Modeling the dynamics of cellular differentiation is fundamental to advancing the understanding and treatment of diseases associated with this process, such as cancer. With the rapid growth of single-cell datasets, this has also become a particularly promising and active domain for machine learning. Current state-of-the-art models, however, rely on computationally expensive optimal transport preprocessing and multi-stage training, while also not discovering explicit gene interactions. To address these challenges we propose Cell-Mechanistic Neural Networks (*Cell-MNN*), an encoder-decoder architecture whose latent representation is a *locally linearized ODE* governing the dynamics of cellular evolution from stem to tissue cells. Cell-MNN is fully end-to-end (besides a standard PCA pre-processing) and its ODE representation explicitly learns biologically consistent and interpretable gene interactions. Empirically, we show that Cell-MNN achieves competitive performance on single-cell benchmarks, surpasses state-of-the-art baselines in scaling to larger datasets and joint training across multiple datasets, while also learning interpretable gene interactions that we validate against the TRRUST database of gene interactions.

1 INTRODUCTION

The process by which stem cells differentiate into specialized tissue cells is poorly understood, and prediction of cellular fate remains an open problem in systems biology. Deeper understanding of the differentiation dynamics is essential for advancing treatment of diseases such as cancer (Chu et al., 2024), neurodegenerative diseases (Cuomo et al., 2023), and to improving wound healing (Rodrigues et al., 2019). While all cells in an organism share the same genome, the level of expression of genes varies over time as differentiation progresses. During this process, genes activate or repress the expression of other genes through complex regulatory mechanisms, causing the cell to differentiate.

Today, only a small subset out of the large number of possible gene interactions has been thoroughly studied. This is due to both the vast combinatorial search space, with $\sim 10^8$ theoretically possible gene interactions, and the experimental effort required to validate specific mechanisms. However, recent advances in single-cell sequencing technology (Macosko et al., 2015; Zheng et al., 2017) have enabled high-throughput measurements that were previously prohibitively expensive, producing datasets that are growing at a pace exceeding Moore's law (Kharchenko, 2021). This rapid growth, coupled with the limitations of direct experimental approaches, presents a unique opportunity to apply machine learning methods to study single-cell dynamics.

In this work we propose Cell-MNN, a method to jointly tackle the challenges of predicting cell fate and discovering gene regulatory interactions. Cell-MNN is an end-to-end encoder-decoder architecture whose representation is a *locally linear* ordinary differential equation (ODE) that governs the dynamics of cellular evolution from stem to tissue cells. The ODE representation of Cell-MNN can learn explicit, biologically consistent, and interpretable gene interactions.

A key challenge in modeling single-cell dynamics is that cells are destroyed by measurement, resulting in datasets that contain a single point along each cell's trajectory (Tong et al., 2020), i.e., a *snapshot observation*. This motivated a line of work on reconstructing trajectories from snapshot data: The best-performing methods in this setting rely on optimal transport (OT) preprocessing to create label trajectories (Tong et al., 2024a; Zhang et al., 2025; Kapusniak et al., 2024; Wang et al., 2025), which becomes a computational bottleneck for large datasets due to quadratic scaling of the

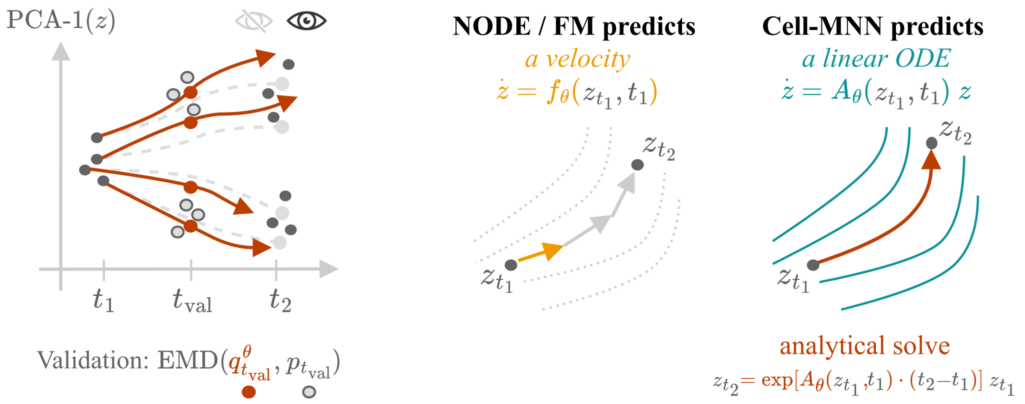
PCA-1(z)
t_1
t_{val}
t_2
Validation: EMD($q^{\theta}_{t_{\text{val}}}$, $p_{t_{\text{val}}}$)
NODE / FM predicts
a velocity
$\dot{z} = f_\theta(z_{t_1}, t_1)$
z_{t_2}
z_{t_1}
Cell-MNN predicts
a linear ODE
$\dot{z} = A_\theta(z_{t_1}, t_1)\, z$
z_{t_2}
z_{t_1}
analytical solve
$z_{t_2} = \exp[A_\theta(z_{t_1}, t_1) \cdot (t_2 - t_1)]\, z_{t_1}$

(a) *Single-cell interpolation problem*

(b) *Difference of Cell-MNN with respect to NODEs*

Figure 1: (**a**) Single-cell interpolation: trajectories are evaluated by the earth mover's distance (EMD) between predictions and the marginal distribution at a held-out time t_{val}. (**b**) Like a hypernetwork, Cell-MNN predicts a linear operator $\boldsymbol{A}_\theta(\boldsymbol{z}, t)$ that approximates the local dynamics explicitly, whereas Neural ODEs (NODE) and Flow Matching (FM) models only output a velocity.

Sinkhorn algorithm with the number of samples (Cuturi, 2013). In contrast, Cell-MNN eliminates OT preprocessing entirely and is designed to be end-to-end. Another bottleneck of state-of-the-art (SOTA) models such as OT-MFM (Kapusniak et al., 2024) and DeepRUOT (Zhang et al., 2025) is that they involve multiple training stages and networks, making amortized training across datasets challenging, whereas Cell-MNN is trained in a single stage, enabling straightforward amortized training across multiple datasets. Furthermore, existing SOTA methods focus primarily on accurate interpolation of empirical distributions and do not learn explicit gene regulatory interactions. By comparison, Cell-MNN learns biologically interpretable interactions through its ODE representation, which explicitly models the interactions governing the predicted cellular evolution. While there are dedicated methods for discovering gene regulatory interactions (Lin et al., 2025), to the best of our knowledge, no such method achieves SOTA predictive performance on single-cell interpolation benchmarks. Cell-MNN addresses both challenges simultaneously, bridging the gap between predictive performance and interpretable gene regulatory modeling.

Contributions. Our main contributions are: (**i**) we propose Cell-MNN, an architecture that models single-cell dynamics via a locally linearized ODE representation; (**ii**) we demonstrate SOTA average performance on three benchmark datasets; (**iii**) we show that eliminating OT preprocessing enables scalability, with Cell-MNN outperforming all baselines on upsampled datasets; (**iv**) we leverage the end-to-end design for amortized training across datasets, surpassing a strong amortized baseline; and (**v**) we exploit the explicit ODE representation to extract gene interactions and quantitatively validate them against the TRRUST database (Han et al., 2018) of gene interactions.

2 Learning the Dynamics of Cells

Formalizing the Problem. We assume a data-generating process consisting of a cell state $\boldsymbol{c}(t) \in \mathcal{C}$ evolving over time in a high-dimensional state space $\mathcal{C}$ that includes all relevant molecular, physical, and biochemical variables, and an observation function mapping this state to data. The measurement process observes only a subset of the full state mapping it to the *gene expression vector* of d_x genes $\boldsymbol{x}_t \in \mathbb{R}^{d_x}$ via an unknown, potentially noisy measurement process $\boldsymbol{m} : \mathcal{C} \to \mathbb{R}^{d_x}$, so that $\boldsymbol{x}(t) = \boldsymbol{m}(\boldsymbol{c}(t))$. Measuring the system involves deconstructing the observed cell, which implies that each measurement corresponds to a single point along its trajectory, i.e., a *snapshot observation*. We assume time $t \in \mathbb{R}$ to be a continuous variable and denote an arbitrary time interval by $\Delta t \in \mathbb{R}$. In practice, the lab schedules a discrete set of experimental time points $\mathcal{T} = \{t_1, t_2, \ldots, t_K\}$ at which cell populations are sampled. We denote by p_t the distribution of $\boldsymbol{x}_t$ at time t. The dataset of snapshot observations is $\mathcal{D} = \{\boldsymbol{x}^{(i)}, t^{(i)}\}_{i=1}^{N}$ with $t^{(i)} \in \mathcal{T}$, and our goal is to learn a best-fit mechanistic model for the dynamics of the observable $\boldsymbol{x}_t$ that is consistent with the family of marginals $\{p_t\}_{t \in \mathcal{T}}$.

2.1 Cell-MNN

SOTA models on single-cell interpolation benchmarks face scalability issues from OT preprocessing and do not learn interpretable gene interactions that can be cross-validated against biological evidence. Our goal is to design a scalable mechanistic model of single-cell dynamics using an ODE representation, enabling accurate forecasting and discovery of interpretable gene interactions.

The Mechanistic Neural Network (MNN) is a recent architecture that Pervez et al. (2024) showed to outperform NeuralODEs on tasks such as solar system dynamics and the n-body problem, while also being able to learn explicit models of the underlying dynamics. This motivates us to design an MNN-inspired architecture for the single-cell setting. However, this domain presents unique challenges that make the vanilla MNN not directly applicable: for ODE discovery, the MNN has only been applied with full trajectories and not yet in biological contexts. Moreover, when identifying a latent space ODE with the MNN, there is typically no way to interpret that ODE in the input space. In contrast, single-cell dynamics require learning latent space dynamics from *snapshot data*. To discover gene interactions, the learned ODE must furthermore be interpretable in the input space. We therefore adapt the MNN architecture to this setting and refer to the resulting version as *Cell-MNN*. Cell-MNN is an encoder–decoder model, learning a mechanistic map

$$\boldsymbol{x}_{t+\Delta t} = \text{Cell-MNN}_\theta(\boldsymbol{x}_t, t, \Delta t),$$

which maps a gene expression vector $\boldsymbol{x}_t$ at time t to a predicted state $\boldsymbol{x}_{t+\Delta t}$ after an *arbitrary* time interval Δt. We define the model-induced distribution at time $t + \Delta t$ as $q^\theta_{t+\Delta t}$, which is the distribution of Cell-MNN$_\theta(\boldsymbol{x}_t, t, \Delta t)$ when $\boldsymbol{x}_t$ is drawn from p_t. As a core part of the architecture, Cell-MNN maps to a compressed representation $\boldsymbol{z} \in \mathbb{R}^{d_z}$, with $d_z \ll d_x$, of the high-dimensional gene expression vector $\boldsymbol{x} \in \mathbb{R}^{d_x}$, and learns the dynamics in the latent space. Following prior work (Tong et al., 2024a), we obtain this latent representation by applying principal component analysis (PCA), with projection matrix $\boldsymbol{V}_{\text{PCA}} \in \mathbb{R}^{d_x \times d_z}$, so that $\boldsymbol{z} = \boldsymbol{V}_{\text{PCA}}^\top \boldsymbol{x}$.

Locally Linearizing the Latent ODE. The latent vector $\boldsymbol{z} \in \mathbb{R}^{d_z}$ in the PCA subspace is assumed to follow non-autonomous, non-linear dynamics $\dot{\boldsymbol{z}} = \boldsymbol{f}(\boldsymbol{z}, t)$. In practice, this ODE is often highly complex, and learning an *explicit* form that globally approximates it would be intractable due to the combinatorial search space of basis functions that grows with increasing latent space dimension d_z.

To address this, we decompose the intractable global ODE discovery problem into smaller subproblems: at the current state $(\boldsymbol{z}^{(i)}, t^{(i)})$, which we also call the *operating point*, we approximate the dynamics by a linear ODE in a small neighborhood. The learning task is then to predict these local dynamics models from the operating point $(\boldsymbol{z}^{(i)}, t^{(i)})$ using an encoder.

$$\begin{aligned}\dot{\boldsymbol{z}} &= \boldsymbol{f}(\boldsymbol{z}, t)\\ &= \boldsymbol{A}(\boldsymbol{z}, t)\, \boldsymbol{z}, \qquad\qquad \text{if } \boldsymbol{f}(\boldsymbol{0}, t) = \boldsymbol{0},\ \forall t \in \mathbb{R},\\ &\approx \boldsymbol{A}_\theta\big(\boldsymbol{z}^{(i)}, t^{(i)}\big)\, \boldsymbol{z}.\end{aligned}$$

We predict the linear operator $\boldsymbol{A}_\theta \in \mathcal{A}$ using a multilayer perceptron $\text{MLP}_\theta : \mathbb{R}^{d_z+1} \to \mathcal{A}$. Here $\mathcal{A} := \mathcal{L}(\mathbb{R}^{d_z}, \mathbb{R}^{d_z}) \cong \mathbb{R}^{d_z \times d_z}$ represents the space of linear operators acting on $\mathbb{R}^{d_z}$. Note that, while the operator governing the local dynamics is linear, it is a non-linear function of the current latent state $\boldsymbol{z}^{(i)}$ and time $t^{(i)}$. In Appendix D, we show that the reparametrization of the right-hand side $\boldsymbol{f}(\boldsymbol{z}, t) = \boldsymbol{A}(\boldsymbol{z}, t)\, \boldsymbol{z}$ always exists under mild assumptions.

This approach is conceptually orthogonal to Neural ODEs (Chen et al., 2018), which learn an *unconditional black-box* approximation to $\boldsymbol{f}$. In the Cell-MNN setting, the MLP functions more like a *hypernetwork* (Ha et al., 2017), outputting a conditional white-box linear function $\boldsymbol{g}_\theta(\boldsymbol{z}, t | \boldsymbol{z}^{(i)}, t^{(i)}) = \boldsymbol{A}_\theta(\boldsymbol{z}^{(i)}, t^{(i)})\, \boldsymbol{z}$ that locally approximates $\boldsymbol{f}$ at the operating point $(\boldsymbol{z}^{(i)}, t^{(i)})$. Unlike most neural operators (Li et al., 2021; Kovachki et al., 2021) that learn a *single* global operator, Cell-MNN predicts a state-conditioned linear operator for each operating point. This makes the learned dynamics explicit and enables amortization across arbitrarily many states and datasets within a single network.

Decoding by Analytically Solving the ODE. Decoding the ODE representation involves solving the ODE system. The locally linearized formulation of the dynamics has the advantage that the latent space ODE admits a local closed-form solution. For fixed $\boldsymbol{A}_\theta$ at the operating point, the system $\dot{\boldsymbol{z}} = \boldsymbol{A}_\theta\, \boldsymbol{z}$ is a linear, time-invariant ODE with solution

$$\boldsymbol{z}(t^{(i)} + \Delta t) = \exp\big(\boldsymbol{A}_\theta \Delta t\big)\, \boldsymbol{z}_t^{(i)}.$$

Predictions in the gene expression space are obtained by projecting back $\boldsymbol{x}(t+\Delta t) = \boldsymbol{V}_{\text{PCA}}\boldsymbol{z}(t+\Delta t)$.

Parametrization of the Operator. For more fine-grained control over the parametrization of $\boldsymbol{A}_\theta$, we let the MLP predict the matrix in an eigen-decomposed form $\boldsymbol{A}_\theta = \boldsymbol{P}_\theta \operatorname{diag}(\boldsymbol{\lambda}_\theta)\, \boldsymbol{P}_\theta^{-1}$, which is also beneficial to compute the matrix exponential. To ensure invertibility of $\boldsymbol{P}_\theta$, we train with the additional regularizer $\mathcal{L}^{\text{inv}}(\theta) = 1/(\det(\boldsymbol{P}_\theta) + \epsilon)$, which is practical if the latent space is small. This also lets us introduce inductive bias by selectively fixing eigenvalues, for example to zero, if needed.

Optimization. We train the MLP parameters θ by minimizing the Maximum Mean Discrepancy (MMD, Gretton et al. (2012))[1] between the model-induced marginals q_t^θ and the empirical marginals μ_t, thereby fitting a mechanistic model whose dynamics align with the target marginals p_t under a future discounting factor γ. All discrepancies are computed in latent space via the pullback kernel

$$k_x(\boldsymbol{x}, \boldsymbol{x}') := k_z\big(\boldsymbol{V}_{\text{PCA}}^\top \boldsymbol{x},\ \boldsymbol{V}_{\text{PCA}}^\top \boldsymbol{x}'\big),$$

so that $\text{MMD}^2(q_t^\theta, p_t; k_x) = \text{MMD}^2(q_t^{\theta,z}, p_t^z; k_z)$. Here, p_t^z and $q_t^{\theta,z}$ denote the distributions of the gene expression marginals in the latent space. The MMD loss is:

$$\mathcal{L}^{\text{MMD}^2}(\theta) = \mathbb{E}_t \left[\sum_{t'=t}^{t_K} \gamma^{t'}\, \text{MMD}^2\big(q_{t'}^\theta, p_{t'}; k_x\big) \right].$$

Following Tong et al. (2020), we also regularize the kinetic energy to improve generalization:

$$\mathcal{L}^{\text{kin}}(\theta) = \mathbb{E}_{t,\, \boldsymbol{z}_t \sim q_t^\theta}\left[\|\dot{\boldsymbol{z}}_t\|^2\right] = \mathbb{E}_{t,\, \boldsymbol{z}_t \sim q_t^\theta}\left[\|\boldsymbol{A}_\theta(\boldsymbol{z}_t, t)\, \boldsymbol{z}_t\|^2\right],$$

which serves as a soft constraint encouraging trajectories close to optimal transport flows in the sense of the Benamou & Brenier (2000) formulation. Our final loss then becomes:

$$\mathcal{L}^{\text{total}}(\theta) = \mathcal{L}^{\text{MMD}^2}(\theta) + \lambda_{\text{kin}}\mathcal{L}^{\text{kin}}(\theta) + \lambda_{\text{inv}}\mathcal{L}^{\text{inv}}(\theta). \tag{1}$$

Computational Complexity. With $\boldsymbol{A}_\theta$ given in eigendecomposed form at an operating point, evaluating the analytical solution (Eq. 2.1) at T time points has time complexity $\mathcal{O}(T\, d_z^2)$ and space complexity $\mathcal{O}(d_z^2)$, where d_z is the latent space dimensionality. This improves the time and space complexity over the Scalable Mechanistic Neural Network (S-MNN) (Chen et al., 2025). Forming the full operator requires computing $\boldsymbol{P}_\theta^{-1}$, incurring a one-time $\mathcal{O}(d_z^3)$ cost per operating point.

Limitations. The cubic time complexity in the latent dimension can become a challenge for high-dimensional latent spaces but could be mitigated by imposing sparsity assumptions on $\boldsymbol{A}_\theta$. In our application to single-cell dynamics, we follow the practice (Tong et al., 2020; 2024a) of using a 5-dimensional PCA space, which we find expressive enough to capture meaningful gene interactions in the high-dimensional gene expression space as presented later in the paper. Note that OT preprocessing on two time points, when using the Sinkhorn algorithm, scales as $\mathcal{O}(d_z\, n^2)$ with the number of samples n, which becomes a bottleneck for large datasets, as n is usually much larger than d_z. However, approximate batch approaches are also possible to address this (Tong et al., 2024a). A separate limitation of predicting the local dynamics is that evolving the system too far may cause it to leave the regime where the linear ODE is accurate, which would require a new forward pass through the encoder to update the ODE. In our experiments, however, we did not encounter this issue.

Uncovering Local Gene Regulatory Interactions. Combining the linear projection to the PCA subspace $\boldsymbol{z} = \boldsymbol{V}_{\text{PCA}}^\top \boldsymbol{x}$ with locally linear dynamics around an operating point $\dot{\boldsymbol{z}} = \boldsymbol{A}_\theta\, \boldsymbol{z}$ enables projecting the predicted local dynamics back into the gene expression space with:

$$\frac{d}{dt}\boldsymbol{z} = \boldsymbol{A}_\theta \boldsymbol{z} \iff \frac{d}{dt}\big(\boldsymbol{V}_{\text{PCA}}^\top \boldsymbol{x}\big) = \boldsymbol{A}_\theta \boldsymbol{V}_{\text{PCA}}^\top \boldsymbol{x} \iff \frac{d}{dt}\boldsymbol{x} = \boldsymbol{V}_{\text{PCA}} \boldsymbol{A}_\theta \boldsymbol{V}_{\text{PCA}}^\top \boldsymbol{x}.$$

which gives direct access to an *explicit* form of the predicted local dynamics in the gene expression space, essentially uncovering the predicted local gene regulatory interactions. We interpret:

$$w_{j\to i}(\boldsymbol{x}, t) := \left[\boldsymbol{V}_{\text{PCA}} \boldsymbol{A}_\theta(\boldsymbol{x}, t) \boldsymbol{V}_{\text{PCA}}^\top\right]_{i,j} \cdot \boldsymbol{x}_j,$$

as the interaction weight of gene j to gene i. It essentially represents the contribution of gene j's expression to the time derivative of $\boldsymbol{x}_i$. This makes our proposed approach fully interpretable, as we can inspect the learned gene interactions directly.

[1] A full definition of the MMD is given in Appendix B

3 Related Works

Single-cell Interpolation. The single-cell trajectory inference problem, as formalized by Lavenant et al. (2023), entails reconstructing continuous dynamics from snapshot data. Early work based on recurrent neural networks (Hashimoto et al., 2016) was followed by NeuralODE-based methods (Tong et al., 2020; 2023; Zhang et al., 2023; Koshizuka & Sato, 2023; Huguet et al., 2022), in which a neural network outputs the velocity field governing the dynamics. In contrast, Cell-MNN predicts an explicit local dynamics model, which not only facilitates the learning of gene interactions but also circumvents the need for numerical ODE solvers.

A separate line of work avoids simulation by relying on OT preprocessing to approximate cell trajectories (Schiebinger et al., 2019; Bunne et al., 2021), which were also used to train flow-matching models such as by Tong et al. (2024a); Kapusniak et al. (2024); Zhang et al. (2025); Wang et al. (2025); Terpin et al. (2024). However, solving the OT coupling with the Sinkhorn algorithm scales quadratically in the number of samples, creating a major bottleneck for large datasets, which is why Tong et al. (2024a) proposed batch-wise approximation. To address this scalability bottleneck, Cell-MNN is designed to eliminate OT preprocessing entirely. Furthermore, SOTA OT-based models such as OT-MFM and DeepRUOT rely on multiple training stages beyond a standard PCA dimensionality reduction, which complicates amortized training across datasets. In contrast, Cell-MNN involves only a single training stage while achieving competitive performance on single-cell benchmarks. Finally, Action Matching (Neklyudov et al., 2023) also avoids OT preprocessing, but unlike Cell-MNN, it does not learn an explicit form of the underlying dynamics.

Gene Regulatory Network Discovery. A complementary line of work assumes that the interactions governing cell differentiation can be represented as a graph, known as a *gene regulatory network* (GRN) (Davidson et al., 2002). Tong et al. (2024b) demonstrated that such GRNs can to some extent be recovered from flow-matching models in the setting of low-dimensional synthetic data as simulated by Pratapa et al. (2020). In contrast, we show that Cell-MNN learns biologically plausible gene interactions directly from *real* single-cell data, validating them against the literature-curated TRRUST database. Additional approaches for GRN discovery include tree-based methods (Huynh-Thu et al., 2010; Moerman et al., 2018), information-theoretic approaches (Chan et al., 2017), regression-based time-series models (Lu et al., 2021), Gaussian processes (Äijö & Lähdesmäki, 2009) and ODE-based models such as PerturbODE (Lin et al., 2025) and SCODE (Matsumoto et al., 2017). However, unlike Cell-MNN, these methods typically learn a static GRN and, to our knowledge, they are either inapplicable to single-cell interpolation benchmarks or do not deliver competitive performance.

Orthogonal to these static GRN approaches, recent methods for *time-resolved* GRN discovery such as Dynamo (Qiu et al., 2022), SCENIC+ (Bravo González-Blas et al., 2023), Marlene (Hasanaj et al., 2025), and Dictys (Wang et al., 2023) infer time-varying GRNs from RNA-velocity or paired scRNA-seq and scATAC-seq data. In contrast, Cell-MNN operates directly on standard scRNA-seq UMI counts from single-cell interpolation benchmarks and yields context-dependent signed interaction weights as a by-product of fitting the dynamics.

ODE Discovery. The idea to learn an explicit ODE representation of the cell differentiation dynamics as pursued by PerturbODE (Lin et al., 2025) and Cell-MNN relates directly to the broader problem of ODE discovery. A seminal method in this area is SINDy (Brunton et al., 2016), which infers governing equations from data but requires access to full trajectories, making it unsuitable for the snapshot-based single-cell setting. Similar limitations apply to more recent approaches such as MNN and related methods such as ODEFormer (Pervez et al., 2024; Chen et al., 2025; Yao et al., 2024; d'Ascoli et al., 2024), which extend ODE discovery to amortized settings by using neural networks to predict the underlying dynamics from observed trajectories. In contrast, Cell-MNN is qualitatively distinct in learning dynamics from population data. It furthermore learns them in *locally linear* form, an idea with strong precedents in physics and control theory such as the Apollo navigation filter (Schmidt, 1966), the control of a 2-link 6-muscle arm model (Li & Todorov, 2004; Todorov & Li, 2005) and rocket landing (Szmuk et al., 2020). The locally linear parameterization theoretically imposes learning control-oriented structure and, in principle, supports the design of performant controllers as described by (Richards et al., 2023), which could enable design of gene perturbations.

Table 1: Model comparison for single-cell interpolation across the *Cite*, *EB*, and *Multi* datasets, sorted by best average performance. We report the mean ± standard deviation of the EMD metric, along with the average across datasets. Standard deviation is computed over left-out time points. Lower values indicate better performance. Values marked * are computed by us.

Method	Cite (5D)	EB (5D)	Multi (5D)	Average ↓
TrajectoryNet (Tong et al., 2020)	–	0.848	–	–
WLF-UOT (Neklyudov et al., 2024)	–	0.800 ±0.002	–	–
NLSB (Koshizuka & Sato, 2023)	–	0.777 ±0.021	–	–
SB-CFM (Tong et al., 2024a)	1.067 ±0.107	1.221 ±0.380	1.129 ±0.363	1.139 ±0.077
[SF]^{2}M-Sink (Tong et al., 2024b)	1.054 ±0.087	1.198 ±0.342	1.098 ±0.308	1.117 ±0.074
[SF]^{2}M-Geo (Tong et al., 2024b)	1.017 ±0.104	0.879 ±0.148	1.255 ±0.179	1.050 ±0.190
I-CFM (Tong et al., 2024a)	0.965 ±0.111	0,872 ±0.087	1.085 ±0.099	0.974 ±0.107
DSB (De Bortoli et al., 2021)	0.965 ±0.111	0.862 ±0.023	1.079 ±0.117	0.969 ±0.109
I-MFM (Kapusniak et al., 2024)	0.916 ±0.124	0.822 ±0.042	1.053 ±0.095	0.930 ±0.116
[SF]^{2}M-Exact (Tong et al., 2024b)	0.920 ±0.049	0.793 ±0.066	0.933 ±0.054	0.882 ±0.077
OT-CFM (Tong et al., 2024a)	0.882 ±0.058	0.790 ±0.068	0.937 ±0.054	0.870 ±0.074
DeepRUOT (Zhang et al., 2025)*	0.845 ±0.167	0.776 ±0.079	0.919 ±0.090	0.846 ±0.071
OT-Interpolate*	0.821 ±0.004	0.749 ±0.019	0.830 ±0.053	0.800 ±0.044
OT-MFM (Kapusniak et al., 2024)	**0.724 ±0.070**	0.713 ±0.039	0.890 ±0.123	0.776 ±0.099
Cell-MNN (ours)*	0.791 ±0.022	**0.690 ±0.073**	**0.742 ±0.100**	**0.741 ±0.050**

4 Experiments

In the following, we present four experiments to evaluate Cell-MNN in terms of predictive accuracy, suitability for amortized training, scalability, and assessment of the predicted gene interactions.

Datasets. For our experiments, we use 3 commonly studied real single-cell datasets. Following Tong et al. (2020), we include the Embryoid Body (*EB*) dataset from Moon et al. (2019), which after preprocessing contains ∼16 K human embryoid cells measured at five time points over 25 days. For EB, we model the time grid with $\mathcal{T} = \{0, 1, ...4\}$. We also use the CITE-seq (*Cite*) and Multiome (*Multi*) datasets from Burkhardt et al. (2022), as repurposed by Tong et al. (2024a). Both consist of gene expression measurements at four time points of cells developing over seven days, with Cite containing ∼31 K cells and Multi ∼33 K cells after preprocessing. Here we model the time grid with the days of measurement, namely $\mathcal{T} = \{0, 1, 2, 3, 7\}$. We use the datasets as preprocessed by Tong et al. (2020; 2024a), which involves filtering for outliers and normalizing the data.

Training. We use the same hyperparameters for all experiments unless stated otherwise. Following Tong et al. (2020), we project gene expression to 5D PCA before training. The MLP used to parameterize $\boldsymbol{A}_\theta$ has depth 4, width 96, leaky ReLU activations, and Kaiming normal initialization (He et al., 2015). For stability, we scale the MLP's last layer by 0.01 at initialization so that predictions of $\boldsymbol{A}_\theta$ start near zero. For the MMD, we use the Laplacian kernel $k(z, z') = \exp[-\frac{\max(||z-z'||_1,\epsilon)}{\sigma \cdot d_z}]$ with parameters $\sigma = 1$ and $\epsilon = 10^{-8}$. We optimize the final loss (Eq. 1) with a batch size per time point of 200, future discount factor $\gamma = 0.1$, initialization scale 0.01, and regularization weights $\lambda_{\text{kin}} = 0.1$ and $\lambda_{\text{inv}} = 1$. Optimization is performed using AdamW (Kingma & Ba, 2017; Loshchilov & Hutter, 2019) with a learning rate of 2×10^{-4} and weight decay 1×10^{-5}. Hyperparameters are selected according to grid search and all experiments are run with three random seeds. We validate every 10 steps, with a patience of 40 validation checks and a maximum training time of 200 minutes. All training runs are performed with one NVIDIA GeForce RTX 2080 Ti per model (11 GB of RAM).

4.1 Single Cell Interpolation

Following Tong et al. (2020; 2024a), we evaluate model performance by measuring how closely it reproduces the marginal distribution of a held-out time point. Each intermediate day is left out in cross-validation fashion to obtain one comprehensive score per dataset.

Metric. For easy comparison with SOTA methods, we follow Tong et al. (2020) and report results in terms of the 1-Wasserstein distance in the PCA subspace (W_1 or otherwise EMD). We use the exact linear programming EMD from the `POT` (Python Optimal Transport) package (Flamary et al., 2021). The EMD metric measures the minimum cost of transporting probability mass to transform one distribution into another, where a lower score represents a closer match of distributions.

Baselines. We compare with the 3 SOTA methods for this task, namely OT-MFM (Kapusniak et al., 2024), OT-CFM (Tong et al., 2024a) and DeepRUOT (Zhang et al., 2025). We found the pre-processing of DeepRUOT to be different from the other approaches, which is why we reran the experiments for DeepRUOT with exactly the same input data as the other methods. We also report the performance of other relevant previous works on this problem as indicated in the results Table 1. As an intuitive bar to cross, we additionally compute the performance of solely interpolating the optimal transport map between two consecutive time points and refer to it as OT-Interpolate.

Results. Table 1 summarizes the results on all three datasets. Cell-MNN achieves the best performance on EB and Multi, and ranks second on Cite, leading to the highest average performance across datasets. Notably, Cell-MNN is the only method that outperforms our proposed OT-Interpolate benchmark on all datasets. We think this is an important additional result, because any method that trains on velocities that are derived from the OT map implicitly treats OT-Interpolate as the ground truth. This also explains the strong performance of OT-Interpolate. Given the above, Cell-MNN delivers highly competitive predictive performance for single-cell interpolation.

4.2 Amortized Training

Model	**Cite** (Inflated)	**EB** (Inflated)	**Multi** (Inflated)
I-CFM	0.0390 ±0.0249	0.0403 ±0.0045	0.0482 ±0.0144
OT-CFM		`-- OOM Error --`	
DeepRUOT		`-- OOM Error --`	
Batch-OT-CFM	0.0232 ±0.0041	0.0243 ±0.0025	0.0302 ±0.0010
Cell-MNN	**0.0225 ±0.0021**	**0.0240 ±0.0039**	**0.0252 ±0.0072**

(a) *Scaling experiment*

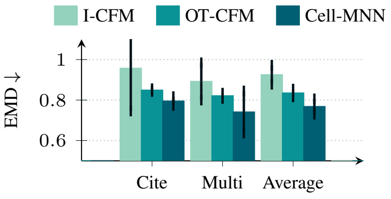

(b) *Amortization experiment*

Figure 2: (**a**) Model comparison across the synthetically inflated datasets. We report mean ± standard deviation of the MMD metric, along with the average across datasets. Lower values indicate better performance. Standard deviation is computed over left-out time points.(**b**) Comparison of models jointly trained on *Cite* and *Multi* datasets to test potential for amortization. We report mean ± standard deviation of the EMD metric, along with the average across datasets.

Foundation models have shown strong transfer learning capabilities across datasets in a variety of domains (Bodnar et al., 2025; Pearce et al., 2025; Bodnar et al., 2025). However, current SOTA methods for single-cell interpolation, such as OT-MFM and DeepRUOT, rely on multi-stage training or dataset-specific regularizers, making them less suitable for building foundation models. In contrast, the end-to-end nature of Cell-MNN enables amortized training across multiple datasets. We design an experiment to assess which models are promising for amortized training in the single-cell interpolation setting by jointly training on datasets with the same time scale, namely Cite and Multi.

Training. Our amortized training setup follows the single-cell interpolation experiment described in Section 4.1, with the only differences being that (i) we iteratively sample batches from Cite and Multi, (ii) we use a wider network with width 128, and (iii) we pass an additional dataset index into the model. We do not sample from the marginals at the left-out time point for either dataset. Since each dataset contains a different set of genes, we use the same PCA embeddings as in the previous experiment (Section 4.1) and merge datasets in the PCA subspace.

Baselines. We use OT-CFM as a baseline as it is the best-performing alternative model on the single-cell interpolation task that involves only a single training stage, making it easy to adapt to the amortized training setting. For each dataset, we compute the OT map on the entire dataset separately to ensure that the derived velocity labels are accurate. We use the hyperparameters specified by Tong et al. (2024a) and first reproduce the original results for the separate-dataset setting to verify our setup. In amortized training, we find that passing the dataset index as input does not affect OT-CFM's performance. For additional reference, we also report the performance of I-CFM.

Results. As shown in Figure 2b, Cell-MNN outperforms both OT-CFM and I-CFM in the amortized setting and achieves performance comparable to training on each dataset separately. Since the gene sets differ between datasets, transfer learning may be difficult in this setup. Nevertheless, these results suggest that for datasets with shared structure, Cell-MNN could enable transfer learning.

4.3 Scalability and Robustness to Noise

Beyond leveraging multiple datasets to train a single model, the practical usefulness of a method depends on its ability to handle the increasingly large datasets available in the single-cell dynamics domain. In this context, performing OT preprocessing over all samples from two consecutive days, as required by OT-CFM, DeepRUOT, or OT-Interpolate, can become a significant bottleneck due to the quadratic time and space complexity of the Sinkhorn algorithm (Cuturi, 2013). To experimentally compare the scalability of different methods, we conduct the following scaling experiment.

Training. We synthetically inflate the dataset size of EB, Cite, and Multi to $250{,}000$ cells each by resampling from each dataset and adding noise drawn from $\mathcal{N}(0, 0.1)$ to the PCA embeddings. Cell-MNN is trained with the same hyperparameters as in our first experiment in Section 4.1.

Baselines. We run OT-CFM and DeepRUOT on the inflated datasets and observe that both methods encounter *out-of-memory* (OOM) errors on our hardware (NVIDIA GeForce RTX 2080 Ti per model, 11 GB RAM) due to the quadratic memory complexity of the Sinkhorn algorithm. To mitigate this, Tong et al. (2024a) proposed a minibatch variant of optimal transport for OT-CFM, which achieves competitive image generation quality compared to dataset-wide OT preprocessing. We therefore use this mini-batch version as a baseline, denoted Batch-OT-CFM. As I-CFM does not require OT preprocessing, we also train it on the inflated datasets and report its performance.

Metric. For the larger datasets, computing the EMD metric becomes impractical, as it also requires estimating the OT map. We therefore use the MMD metric with a Laplacian kernel to compute the validation score. Since MMD can be computed in a batch-wise fashion, it is more practical for this experiment. We use the same hyperparameters for the MMD metric as for the training loss.

Results. We present the validation scores for models trained on inflated datasets in Table 2a. Performing dataset-wide OT preprocessing, as required by standard OT-CFM or DeepRUOT, leads to OOM errors due to the quadratic space complexity of the Sinkhorn algorithm. Batch-OT-CFM outperforms I-CFM, demonstrating the gains from minibatch OT. However, Cell-MNN achieves the best performance on all three inflated datasets, highlighting its scalability and robustness to noise.

4.4 Discovering Gene Interactions

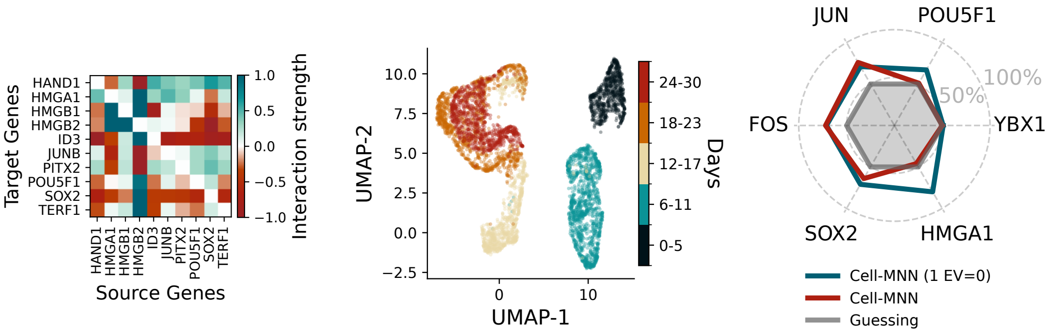

(a) *Gene interactions* (b) *UMAP of operators* (c) *F1 Score on TRRUST*

Figure 3: (**a**) Strongest predicted gene interactions by Cell-MNN for days 12–17 of the EB dataset, normalized to the range $[-1, 1]$. (**b**) UMAP projection of operators predicted by Cell-MNN on the EB dataset, showing that the model learns distinct dynamics at different time points. (**c**) Validation of predicted gene interactions by two Cell-MNN versions: For each source gene j, we classify each TRRUST edge $j \to i$ as activating or repressing using the sign of Cell-MNN's learned weight $w_{j\to i}$.

Cell-MNN predicts the local dynamics of the cell differentiation process in gene expression space, thereby learning interaction weights $w_{j\to i}$ from each gene to every other gene as described in Section 2.1. This corresponds to unsupervised learning of local gene interactions. To assess whether these learned interactions are biologically meaningful, we validate them against the literature-curated TRRUST database (Han et al., 2018), which contains 8,444 regulatory relationships synthe-

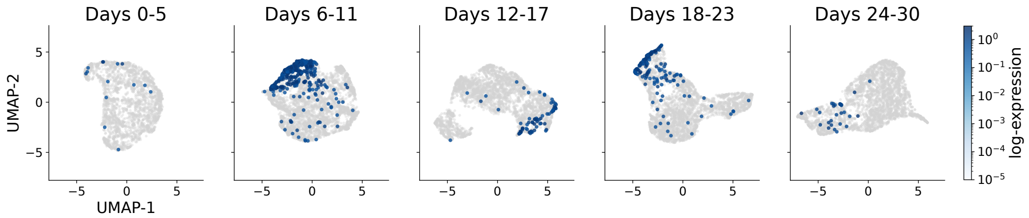

Figure 4: UMAPs of the predicted operators by Cell-MNN across the five time ranges of EB. Points are colored by whether joint expression of the EN-1 marker genes *FOXA2* and *SOX17* is above the 95th percentile. Clustering indicates that Cell-MNN learns distinct dynamics for the EN-1 cell type.

Table 2: GRN discovery on the EB dataset (F1 score in %). For each source gene we report the F1 score of predicting activation vs. repression for labeled TRRUST interactions. Best method per row is highlighted in bold. Performance is averaged over three seeds for OT-CFM and Cell-MNN.

Source gene	**# Labeled interactions**	**SCODE**	**OT-CFM (J)**	**Cell-MNN (1EV=0)**
JUN	65	56.34%	64% ±2%	**71%** ±6%
FOS	25	38.10%	50% ±6%	**71%** ±10%
YBX1	24	54.55%	**72%** ±4%	51% ±6%
POU5F1	19	14.29%	13% ±1%	**67%** ±6%
SOX2	16	**84.21%**	60% ±0%	71% ±9%
HMGA1	10	25.00%	31% ±9%	**80%** ±6%
Average		46.32% ±25.09%	55% ±22.46%	**71%** ±9.50%

sized from 11,237 PubMed articles. While TRRUST represents only a small subset of all potential relationships, it provides a valuable reference signal for evaluating Cell-MNN's predictions.

Unsupervised Classification. Using labels from the TRRUST database, we design an *unsupervised* classification task for a source gene j: for every interaction $j \to i$ listed in TRRUST, we predict whether the relationship is activating or repressing. Since Cell-MNN outputs $w_{j\to i}$ per cell, we average these values over the dataset to obtain a single prediction for each interaction, classifying it as activating if $\sum_{(\boldsymbol{x},t)\in\mathcal{D}} w_{j\to i}(\boldsymbol{x},t) > 0$ and repressing if smaller than zero. We report results for the genes j that are in the top 10 most active ones (as by summing over all interaction weights per gene) for any time point and that have more than 10 matching TRRUST interactions within the EB gene set.

Training and Inductive Bias. We train an ensemble of Cell-MNN models for single-cell interpolation on EB, each with a different left-out marginal. The setup matches Section 4.1 but uses a less preprocessed EB version, retaining gene names for downstream interaction analysis. To highlight the benefit of having access to an explicit dynamics model, we also introduce an additional model version with inductive bias on the parametrization of the linear operator $\boldsymbol{A}_\theta$: in particular, we know that only some genes vary over time, implying that at least one eigenvalue of $\boldsymbol{A}_\theta$ should be zero. During training, we therefore fix one eigenvalue to zero, forcing the model to learn static directions in the gene expression space. While this inductive bias reduces predictive performance in the single-cell interpolation setting by approximately 1%, it significantly improves gene interaction discovery performance on TRRUST (see Appendix 8 for ablation results).

Baselines. To contextualize the results, we restrict our comparison to approaches that predict *signed* GRNs, as this is required for our classification task. As an ODE-based baseline, we run SCODE (Matsumoto et al., 2017) on the dataset. To compare with the idea of using the Jacobian of Neural ODEs as a proxy for the GRN (Qiu et al., 2022), we compute the Jacobians of a fully trained OT-CFM model (OT-CFM (J)). This can be thought of as an alternative to the operators predicted by Cell-MNN. Similar to Cell-MNN, we use the sign of the Jacobian to classify an interaction as activating or repressing. Given different models, we only adapt the GRN prediction in our pipeline; the rest of the evaluation remains the same.

Results. We compute precision, recall, and F1 scores for the *unsupervised* classification task, with results presented in Figure 3 with all numerical values in Table 5 and 6. For all but two of the source genes, the vanilla Cell-MNN achieves better-than-average performance, indicating that for the tested gene regulatory interactions, the model can meaningfully discover activation or repression in a fully unsupervised manner. Interestingly, the Cell-MNN variant with one eigenvalue set to zero significantly improves classification performance, demonstrating that the inductive bias introduced on the operator effectively constrains the solution space. Note that gene interactions are context-dependent (e.g., varying by cell type or other factors), and therefore the labels in TRRUST may not fully apply to the context of the EB dataset. Nevertheless, we view the agreement for the most dominant source genes as a meaningful signal that the mechanisms learned by Cell-MNN are biologically plausible.

Visualizing Operators. To visualize the learned operators, we plot UMAP projections of $\boldsymbol{A}_\theta$ computed jointly across all time ranges (Figure 3b) and separately for each time range (Figure 4) in the EB dataset. The joint projection shows that Cell-MNN captures distinct dynamics across time, while the separate projections highlight differences between cell types. Additional UMAP visualizations for the cell types reported in the original EB study (Moon et al., 2019) are provided in Appendix G.

5 Conclusion

We introduced Cell-MNN, an encoder-decoder architecture whose representation is a locally linear latent ODE at the operating point of the cell differentiation dynamics. The formulation explicitly captures gene interactions conditioned on the time and gene expression. Empirically, we show that Cell-MNN achieves competitive performance on single-cell benchmarks, as well as in scaling and amortization experiments. Importantly, the gene interactions learned from real single-cell data exhibit consistency with the literature-curated TRRUST database. Thus, Cell-MNN jointly addresses the challenges of trajectory reconstruction from snapshot data and gene interaction discovery.

Having shown that Cell-MNN learns biologically plausible gene interactions, a natural next step is to use it as a hypothesis generation engine for less-studied genes, guiding which interactions to test experimentally. Moreover, since Cell-MNN models dynamics in locally linear form, it may be possible to leverage the rich control theory literature on controller design for such locally linear systems. In principle, this could enable steering gene expression states toward desired configurations via perturbations, which could for example inform CRISPR-based gene edits (Jinek et al., 2012).

6 Ethics Statement

All datasets used in this work (EB, Cite, Multi) are publicly available and were preprocessed by prior works Tong et al. (2024a; 2020). While the gene regulatory interactions predicted by Cell-MNN are partially validated against the TRRUST database, they should not be interpreted as definitive biological ground truth without further experimental validation. It is important to note that the model provides hypotheses for experimental follow-up, not direct medical recommendations. Insights from the model could eventually inform gene perturbation studies or therapeutic research. To mitigate potential misuse, we emphasize that the work is intended for advancing computational methodology in machine learning and computational biology, not for direct clinical application. We provide code and hyperparameters for reproducibility.

7 Reproducibility

We use the datasets in the form as preprocessed by prior work: Cite and Multi from Tong et al. (2024a)[2] and EB from Tong et al. (2020)[3]. For the gene discovery experiment, we use the less preprocessed version of EB provided by Tong et al. (2024a). All experiments are run on a single GPU and hyperparameters are presented in Table 3 in the Appendix together with the hardware and training time. We fix random seeds and report all results averaged over three runs with different seeds. Anonymous code is included with the submission as a zip archive, containing environment specifications in `environment.yml`. Commands to reproduce results are documented in the accompanying `README.md`. We will release the full codebase publicly upon publication.

[2] https://data.mendeley.com/datasets/hhny5ff7yj/1

[3] https://github.com/KrishnaswamyLab/TrajectoryNet/tree/master/data

REFERENCES

Jean-David Benamou and Yann Brenier. A computational fluid mechanics solution to the monge-kantorovich mass transfer problem. *Numerische Mathematik*, 84(3):375–393, 2000. URL https://doi.org/10.1007/s002110050002.

Cristian Bodnar, Wessel P. Bruinsma, Ana Lucic, Megan Stanley, Anna Allen, Johannes Brandstetter, Patrick Garvan, Maik Riechert, Jonathan A. Weyn, Haiyu Dong, Jayesh K. Gupta, Kit Thambiratnam, Alexander T. Archibald, Chun-Chieh Wu, Elizabeth Heider, Max Welling, Richard E. Turner, and Paris Perdikaris. A foundation model for the earth system. *Nature*, 641(8065):1180–1187, 2025. URL https://doi.org/10.1038/s41586-025-09005-y.

Carmen Bravo González-Blas, Seppe De Winter, Gert Hulselmans, Nikolai Hecker, Irina Matetovici, Valerie Christiaens, Suresh Poovathingal, Jasper Wouters, Sara Aibar, and Stein Aerts. Scenic+: single-cell multiomic inference of enhancers and gene regulatory networks. *Nature Methods*, 20 (9):1355–1367, 2023.

Steven L. Brunton, Joshua L. Proctor, and J. Nathan Kutz. Discovering governing equations from data by sparse identification of nonlinear dynamical systems. *Proceedings of the National Academy of Sciences*, 113(15):3932–3937, 2016. URL https://www.pnas.org/doi/abs/10.1073/pnas.1517384113.

Charlotte Bunne, Laetitia Meng-Papaxanthos, Andreas Krause, and Marco Cuturi. Jkonet: Proximal optimal transport modeling of population dynamics. *CoRR*, 2021. URL https://arxiv.org/abs/2106.06345.

Daniel Burkhardt, Malte Luecken, Andrew Benz, Peter Holderrieth, Jonathan Bloom, Christopher Lance, Ashley Chow, and Ryan Holbrook. Open problems - multimodal single-cell integration. https://kaggle.com/competitions/open-problems-multimodal, 2022. Kaggle.

Thalia E. Chan, Michael P.H. Stumpf, and Ann C. Babtie. Gene regulatory network inference from single-cell data using multivariate information measures. *Cell Systems*, 5(3):251–267.e3, 2017. ISSN 2405-4712. URL https://www.sciencedirect.com/science/article/pii/S2405471217303861.

Jiale Chen, Dingling Yao, Adeel Pervez, Dan Alistarh, and Francesco Locatello. Scalable mechanistic neural networks. In *The Thirteenth International Conference on Learning Representations*, 2025. URL https://openreview.net/forum?id=Oazgf8A24z.

Ricky T. Q. Chen, Yulia Rubanova, Jesse Bettencourt, and David K Duvenaud. Neural ordinary differential equations. In S. Bengio, H. Wallach, H. Larochelle, K. Grauman, N. Cesa-Bianchi, and R. Garnett (eds.), *Advances in Neural Information Processing Systems*, volume 31, 2018. URL https://proceedings.neurips.cc/paper_files/paper/2018/file/69386f6bb1dfed68692a24c8686939b9-Paper.pdf.

Xianjing Chu, Wentao Tian, Jiaoyang Ning, Gang Xiao, Yunqi Zhou, Ziqi Wang, Zhuofan Zhai, Guilong Tanzhu, Jie Yang, and Rongrong Zhou. Cancer stem cells: advances in knowledge and implications for cancer therapy. *Signal Transduction and Targeted Therapy*, 9(1):170, 2024. ISSN 2059-3635. URL https://doi.org/10.1038/s41392-024-01851-y.

Anna S. E. Cuomo, Aparna Nathan, Soumya Raychaudhuri, Daniel G. MacArthur, and Joseph E. Powell. Single-cell genomics meets human genetics. *Nature Reviews Genetics*, 24(8):535–549, August 2023. ISSN 1471-0064. URL https://doi.org/10.1038/s41576-023-00599-5.

Marco Cuturi. Sinkhorn distances: Lightspeed computation of optimal transport. In *Advances in Neural Information Processing Systems*, volume 26, 2013. URL https://proceedings.neurips.cc/paper_files/paper/2013/file/af21d0c97db2e27e13572cbf59eb343d-Paper.pdf.

Stéphane d'Ascoli, Sören Becker, Philippe Schwaller, Alexander Mathis, and Niki Kilbertus. ODEFormer: Symbolic regression of dynamical systems with transformers. In *The Twelfth International Conference on Learning Representations*, 2024. URL `https://openreview.net/forum?id=TzoHLiGVMo`.

Eric H. Davidson, Jonathan P. Rast, Paola Oliveri, Andrew Ransick, Cristina Calestani, Chiou-Hwa Yuh, Takuya Minokawa, Gabriele Amore, Veronica Hinman, Cesar Arenas-Mena, Ochan Otim, C. Titus Brown, Carolina B. Livi, Pei Yun Lee, Roger Revilla, Alistair G. Rust, Zheng Jun Pan, Maria J. Schilstra, Peter J. C. Clarke, Maria I. Arnone, Lee Rowen, R. Andrew Cameron, David R. McClay, Leroy Hood, and Hamid Bolouri. A genomic regulatory network for development. *Science*, 295(5560):1669–1678, 2002.

Valentin De Bortoli, James Thornton, Jeremy Heng, and Arnaud Doucet. Diffusion schrödinger bridge with applications to score-based generative modeling. In M. Ranzato, A. Beygelzimer, Y. Dauphin, P.S. Liang, and J. Wortman Vaughan (eds.), *Advances in Neural Information Processing Systems*, volume 34, pp. 17695–17709, 2021. URL `https://proceedings.neurips.cc/paper_files/paper/2021/file/940392f5f32a7ade1cc201767cf83e31-Paper.pdf`.

Rémi Flamary, Nicolas Courty, Alexandre Gramfort, Mokhtar Z. Alaya, AurÃ©lie Boisbunon, Stanislas Chambon, Laetitia Chapel, Adrien Corenflos, Kilian Fatras, Nemo Fournier, LÃ©o Gautheron, Nathalie T.H. Gayraud, Hicham Janati, Alain Rakotomamonjy, Ievgen Redko, Antoine Rolet, Antony Schutz, Vivien Seguy, Danica J. Sutherland, Romain Tavenard, Alexander Tong, and Titouan Vayer. Pot: Python optimal transport. *Journal of Machine Learning Research*, 22(78):1–8, 2021. URL `http://jmlr.org/papers/v22/20-451.html`.

Arthur Gretton, Karsten M. Borgwardt, Malte J. Rasch, Bernhard Schölkopf, and Alexander Smola. A kernel two-sample test. *Journal of Machine Learning Research*, 13(25):723–773, 2012. URL `http://jmlr.org/papers/v13/gretton12a.html`.

David Ha, Andrew M. Dai, and Quoc V. Le. Hypernetworks. In *International Conference on Learning Representations*, 2017. URL `https://openreview.net/forum?id=rkpACe1lx`.

Heonjong Han, Jae-Won Cho, Sangyoung Lee, Ayoung Yun, Hyojin Kim, Dasom Bae, Sunmo Yang, Chan Yeong Kim, Muyoung Lee, Eunbeen Kim, Sungho Lee, Byunghee Kang, Dabin Jeong, Yaeji Kim, Hyeon-Nae Jeon, Haein Jung, Sunhwee Nam, Michael Chung, Jong-Hoon Kim, and Insuk Lee. TRRUST v2: an expanded reference database of human and mouse transcriptional regulatory interactions. *Nucleic Acids Research*, 46(D1):D380–D386, January 2018. ISSN 1362-4962. URL `https://doi.org/10.1093/nar/gkx1013`.

Euxhen Hasanaj, Barnabás Póczos, and Ziv Bar-Joseph. Recovering time-varying networks from single-cell data. *Bioinformatics*, 41(Supplement_1):i628–i636, 07 2025.

Tatsunori Hashimoto, David Gifford, and Tommi Jaakkola. Learning population-level diffusions with generative rnns. Proceedings of Machine Learning Research, pp. 2417–2426, New York, New York, USA, 20–22 Jun 2016. PMLR. URL `https://proceedings.mlr.press/v48/hashimoto16.html`.

Kaiming He, Xiangyu Zhang, Shaoqing Ren, and Jian Sun. Delving deep into rectifiers: Surpassing human-level performance on imagenet classification. In *Proceedings of the IEEE International Conference on Computer Vision (ICCV)*, December 2015.

Guillaume Huguet, D. S. Magruder, Alexander Tong, Oluwadamilola Fasina, Manik Kuchroo, Guy Wolf, and Smita Krishnaswamy. Manifold interpolating optimal-transport flows for trajectory inference, 2022. URL `https://arxiv.org/abs/2206.14928`.

Vân Anh Huynh-Thu, Alexandre Irrthum, Louis Wehenkel, and Pierre Geurts. Inferring regulatory networks from expression data using tree-based methods. 5(9):1–10, 09 2010. URL `https://doi.org/10.1371/journal.pone.0012776`.

Martin Jinek, Krzysztof Chylinski, Ines Fonfara, Michael Hauer, Jennifer A. Doudna, and Emmanuelle Charpentier. A programmable dual-rna-guided dna endonuclease in adaptive bacterial immunity. *Science*, 337(6096):816–821, 2012.

Kacper Kapusniak, Peter Potaptchik, Teodora Reu, Leo Zhang, Alexander Tong, Michael M. Bronstein, Joey Bose, and Francesco Di Giovanni. Metric flow matching for smooth interpolations on the data manifold. In *The Thirty-eighth Annual Conference on Neural Information Processing Systems*, 2024. URL https://openreview.net/forum?id=fE3RqiF4Nx.

Peter V. Kharchenko. The triumphs and limitations of computational methods for scrna-seq. *Nature Methods*, 18(7):723–732, 2021. URL https://doi.org/10.1038/s41592-021-01171-x.

Diederik P. Kingma and Jimmy Ba. Adam: A method for stochastic optimization, 2017. URL https://arxiv.org/abs/1412.6980.

Takeshi Koshizuka and Issei Sato. Neural lagrangian schrödinger bridge: Diffusion modeling for population dynamics. In *ICLR*, 2023. URL https://openreview.net/forum?id=d3QNWD_pcFv.

Nikola B. Kovachki, Zongyi Li, Burigede Liu, Kamyar Azizzadenesheli, Kaushik Bhattacharya, Andrew M. Stuart, and Anima Anandkumar. Neural operator: Learning maps between function spaces. *CoRR*, 2021. URL https://arxiv.org/abs/2108.08481.

Hugo Lavenant, Stephen Zhang, Young-Heon Kim, and Geoffrey Schiebinger. Towards a mathematical theory of trajectory inference, 2023. URL https://arxiv.org/abs/2102.09204.

Weiwei Li and Emanuel Todorov. Iterative linear quadratic regulator design for nonlinear biological movement systems. In *Proceedings of the 1st International Conference on Informatics in Control, Automation and Robotics, (ICINCO 2004)*, volume 1, pp. 222–229, 01 2004.

Zongyi Li, Nikola Borislavov Kovachki, Kamyar Azizzadenesheli, Burigede liu, Kaushik Bhattacharya, Andrew Stuart, and Anima Anandkumar. Fourier neural operator for parametric partial differential equations. In *International Conference on Learning Representations*, 2021. URL https://openreview.net/forum?id=c8P9NQVtmnO.

Zaikang Lin, Sei Chang, Aaron Zweig, Minseo Kang, Elham Azizi, and David A. Knowles. Interpretable neural odes for gene regulatory network discovery under perturbations, 2025. URL https://arxiv.org/abs/2501.02409.

Ilya Loshchilov and Frank Hutter. Decoupled weight decay regularization. In *International Conference on Learning Representations*, 2019. URL https://openreview.net/forum?id=Bkg6RiCqY7.

Jonathan Lu, Bianca Dumitrascu, Ian C. McDowell, Brian Jo, Alejandro Barrera, Linda K. Hong, Sarah M. Leichter, Timothy E. Reddy, and Barbara E. Engelhardt. Causal network inference from gene transcriptional time-series response to glucocorticoids. *PLOS Computational Biology*, 17 (1):1–29, 01 2021. URL https://doi.org/10.1371/journal.pcbi.1008223.

Evan Z. Macosko, Anindita Basu, Rahul Satija, James Nemesh, Karthik Shekhar, Melissa Goldman, Itay Tirosh, Allison R. Bialas, Nolan Kamitaki, Emily M. Martersteck, John J. Trombetta, David A. Weitz, Joshua R. Sanes, Alex K. Shalek, Aviv Regev, and Steven A. McCarroll. Highly parallel genome-wide expression profiling of individual cells using nanoliter droplets. *Cell*, 161 (5):1202–1214, 2015. URL https://doi.org/10.1016/j.cell.2015.05.002.

Hirotaka Matsumoto, Hisanori Kiryu, Chikara Furusawa, Minoru S H Ko, Shigeru B H Ko, Norio Gouda, Tetsutaro Hayashi, and Itoshi Nikaido. Scode: an efficient regulatory network inference algorithm from single-cell rna-seq during differentiation. *Bioinformatics*, 33(15):2314–2321, 04 2017. URL https://doi.org/10.1093/bioinformatics/btx194.

Thomas Moerman, Sara Aibar Santos, Carmen Bravo González-Blas, Jaak Simm, Yves Moreau, Jan Aerts, and Stein Aerts. Grnboost2 and arboreto: efficient and scalable inference of gene regulatory networks. *Bioinformatics*, 35(12):2159–2161, 11 2018. ISSN 1367-4803. URL https://doi.org/10.1093/bioinformatics/bty916.

Kevin R. Moon, David van Dijk, Zheng Wang, Scott Gigante, Daniel B. Burkhardt, William S. Chen, Kristina Yim, Antonia van den Elzen, Matthew J. Hirn, Ronald R. Coifman, Natalia B. Ivanova, Guy Wolf, and Smita Krishnaswamy. Visualizing structure and transitions in high-dimensional biological data. *Nature Biotechnology*, 37(12):1482–1492, 2019. URL https://nature.com/articles/s41587-019-0336-3.

Kirill Neklyudov, Rob Brekelmans, Daniel Severo, and Alireza Makhzani. Action matching: Learning stochastic dynamics from samples. In Andreas Krause, Emma Brunskill, Kyunghyun Cho, Barbara Engelhardt, Sivan Sabato, and Jonathan Scarlett (eds.), *Proceedings of the 40th International Conference on Machine Learning*, volume 202 of *Proceedings of Machine Learning Research*, pp. 25858–25889. PMLR, 23–29 Jul 2023. URL https://proceedings.mlr.press/v202/neklyudov23a.html.

Kirill Neklyudov, Rob Brekelmans, Alexander Tong, Lazar Atanackovic, Qiang Liu, and Alireza Makhzani. A computational framework for solving wasserstein lagrangian flows. In *ICML*, 2024. URL https://openreview.net/forum?id=wwItuHdus6.

James D Pearce, Sara E Simmonds, Gita Mahmoudabadi, Lakshmi Krishnan, Giovanni Palla, Ana-Maria Istrate, Alexander Tarashansky, Benjamin Nelson, Omar Valenzuela, Donghui Li, Stephen R Quake, and Theofanis Karaletsos. A cross-species generative cell atlas across 1.5 billion years of evolution: The transcriptformer single-cell model. *bioRxiv*, 2025. URL https://www.biorxiv.org/content/early/2025/04/29/2025.04.25.650731.

Adeel Pervez, Francesco Locatello, and Stratis Gavves. Mechanistic neural networks for scientific machine learning. In *Forty-first International Conference on Machine Learning*, 2024. URL https://openreview.net/forum?id=pLtuwhoQh7.

Aditya Pratapa, Amogh P. Jalihal, Jeffrey N. Law, Aditya Bharadwaj, and T. M. Murali. Benchmarking algorithms for gene regulatory network inference from single-cell transcriptomic data. *Nature Methods*, 17(2):147–154, 2020. URL https://doi.org/10.1038/s41592-019-0690-6.

Xiaojie Qiu, Yan Zhang, Jorge D. Martin-Rufino, Chen Weng, Shayan Hosseinzadeh, Dian Yang, Angela N. Pogson, Marco Y. Hein, Kyung Hoi (Joseph) Min, Li Wang, Emanuelle I. Grody, Matthew J. Shurtleff, Ruoshi Yuan, Song Xu, Yian Ma, Joseph M. Replogle, Eric S. Lander, Spyros Darmanis, Ivet Bahar, Vijay G. Sankaran, Jianhua Xing, and Jonathan S. Weissman. Mapping transcriptomic vector fields of single cells. *Cell*, 185(4):690–711.e45, 2022.

Spencer M. Richards, Jean-Jacques Slotine, Navid Azizan, and Marco Pavone. Learning control-oriented dynamical structure from data. In Andreas Krause, Emma Brunskill, Kyunghyun Cho, Barbara Engelhardt, Sivan Sabato, and Jonathan Scarlett (eds.), *Proceedings of the 40th International Conference on Machine Learning*, volume 202 of *Proceedings of Machine Learning Research*, pp. 29051–29062. PMLR, 23–29 Jul 2023. URL https://proceedings.mlr.press/v202/richards23a.html.

Melanie Rodrigues, Nina Kosaric, Clark A. Bonham, and Geoffrey C. Gurtner. Wound healing: A cellular perspective. *Physiological Reviews*, 99(1):665–706, 2019. URL https://doi.org/10.1152/physrev.00067.2017.

Geoffrey Schiebinger, Jian Shu, Marcin Tabaka, Brian Cleary, Vidya Subramanian, Aryeh Solomon, Joshua Gould, Siyan Liu, Stacie Lin, Peter Berube, Lia Lee, Jenny Chen, Justin Brumbaugh, Philippe Rigollet, Konrad Hochedlinger, Rudolf Jaenisch, Aviv Regev, and Eric S. Lander. Optimal-transport analysis of single-cell gene expression identifies developmental trajectories in reprogramming. *Cell*, 176(4):928–943.e22, 2019. URL https://www.sciencedirect.com/science/article/pii/S009286741930039X.

Stanley F. Schmidt. Application of state-space methods to navigation problems. volume 3 of *Advances in Control Systems*, pp. 293–340. Elsevier, 1966. URL https://www.sciencedirect.com/science/article/pii/B9781483167169500114.

Michael Szmuk, Taylor P. Reynolds, and Behçet Açıkmeşe. Successive convexification for real-time six-degree-of-freedom powered descent guidance with state-triggered constraints. *Journal* *of Guidance, Control, and Dynamics*, 43(8):1399–1413, 2020. URL https://doi.org/10.2514/1.G004549.

Antonio Terpin, Nicolas Lanzetti, Martín Gadea, and Florian Dorfler. Learning diffusion at lightspeed. In *The Thirty-eighth Annual Conference on Neural Information Processing Systems*, 2024. URL https://openreview.net/forum?id=y10avdRFNK.

Emanuel Todorov and Weiwei Li. A generalized iterative lqg method for locally-optimal feedback control of constrained nonlinear stochastic systems. In *Proceedings of the 2005, American Control Conference, 2005.*, pp. 300–306 vol. 1, 2005.

Alexander Tong, Jessie Huang, Guy Wolf, David Van Dijk, and Smita Krishnaswamy. TrajectoryNet: A dynamic optimal transport network for modeling cellular dynamics. In Hal Daumé III and Aarti Singh (eds.), *Proceedings of the 37th International Conference on Machine Learning*, volume 119 of *Proceedings of Machine Learning Research*, pp. 9526–9536. PMLR, 13–18 Jul 2020. URL https://proceedings.mlr.press/v119/tong20a.html.

Alexander Tong, Manik Kuchroo, Shabarni Gupta, Aarthi Venkat, Beatriz P. San Juan, Laura Rangel, Brandon Zhu, John G. Lock, Christine L. Chaffer, and Smita Krishnaswamy. Learning transcriptional and regulatory dynamics driving cancer cell plasticity using neural ode-based optimal transport. *bioRxiv*, 2023. URL https://www.biorxiv.org/content/early/2023/03/29/2023.03.28.534644.

Alexander Tong, Kilian Fatras, Nikolay Malkin, Guillaume Huguet, Yanlei Zhang, Jarrid Rector-Brooks, Guy Wolf, and Yoshua Bengio. Improving and generalizing flow-based generative models with minibatch optimal transport. *Transactions on Machine Learning Research*, 2024a. URL https://openreview.net/forum?id=CD9Snc73AW. Expert Certification.

Alexander Tong, Nikolay Malkin, Kilian Fatras, Lazar Atanackovic, Yanlei Zhang, Guillaume Huguet, Guy Wolf, and Yoshua Bengio. Simulation-free schrödinger bridges via score and flow matching. In *AISTATS*, pp. 1279–1287, 2024b. URL https://proceedings.mlr.press/v238/y-tong24a.html.

Dongyi Wang, Yuanwei Jiang, Zhenyi Zhang, Xiang Gu, Peijie Zhou, and Jian Sun. Joint velocity-growth flow matching for single-cell dynamics modeling, 2025. URL https://arxiv.org/abs/2505.13413.

Lingfei Wang, Nikolaos Trasanidis, Ting Wu, Guanlan Dong, Michael Hu, Daniel E. Bauer, and Luca Pinello. Dictys: dynamic gene regulatory network dissects developmental continuum with single-cell multiomics. *Nature Methods*, 20(9):1368–1378, 2023.

Dingling Yao, Caroline Muller, and Francesco Locatello. Marrying causal representation learning with dynamical systems for science. In *The Thirty-eighth Annual Conference on Neural Information Processing Systems*, 2024. URL https://openreview.net/forum?id=MWHRxKz4mq.

Jiaqi Zhang, Erica Larschan, Jeremy Bigness, and Ritambhara Singh. scnode : Generative model for temporal single cell transcriptomic data prediction. *bioRxiv*, 2023. URL https://www.biorxiv.org/content/early/2023/11/23/2023.11.22.568346.

Zhenyi Zhang, Tiejun Li, and Peijie Zhou. Learning stochastic dynamics from snapshots through regularized unbalanced optimal transport. In *The Thirteenth International Conference on Learning Representations*, 2025. URL https://openreview.net/forum?id=gQlxd3Mtru.

Grace X. Y. Zheng, Jessica M. Terry, Phillip Belgrader, Paul Ryvkin, Zachary W. Bent, Ryan Wilson, Solongo B. Ziraldo, Tobias D. Wheeler, Geoff P. McDermott, Junjie Zhu, Mark T. Gregory, Joe Shuga, Luz Montesclaros, Jason G. Underwood, Donald A. Masquelier, Stefanie Y. Nishimura, Michael Schnall-Levin, Paul W. Wyatt, Christopher M. Hindson, Rajiv Bharadwaj, Alexander Wong, Kevin D. Ness, Lan W. Beppu, H. Joachim Deeg, Christopher McFarland, Keith R. Loeb, William J. Valente, Nolan G. Ericson, Emily A. Stevens, Jerald P. Radich, Tarjei S. Mikkelsen, Benjamin J. Hindson, and Jason H. Bielas. Massively parallel digital transcriptional profiling of single cells. *Nature Communications*, 8(1):14049, 2017. URL https://doi.org/10.1038/ncomms14049.

Tarmo Äijö and Harri Lähdesmäki. Learning gene regulatory networks from gene expression measurements using non-parametric molecular kinetics. *Bioinformatics*, 25(22):2937–2944, 08 2009. URL `https://doi.org/10.1093/bioinformatics/btp511`.

Tayfun Çimen. Systematic and effective design of nonlinear feedback controllers via the state-dependent riccati equation (sdre) method. *Annual Reviews in Control*, 34(1):32–51, 2010. URL `https://www.sciencedirect.com/science/article/pii/S1367578810000052`.

A USE OF LARGE LANGUAGE MODELS (LLMS)

In this work, we used LLMs for (i) coding assistance during the software development phase, (ii) identifying relevant literature in response to specific research questions, and (iii) polishing and improving the readability of the paper. All substantive research contributions, analysis, and interpretations were carried out by the authors.

B DEFINITIONS

Maximum Mean Discrepancy (MMD, Gretton et al. (2012)): Given two distributions p and q over $\mathcal{X}$ and a positive-definite kernel function $k : \mathcal{X} \times \mathcal{X} \to \mathbb{R}$, the squared Maximum Mean Discrepancy (MMD) is defined as

$$\mathrm{MMD}^2(p, q; k) = \mathbb{E}_{x,x'\sim p}[k(x, x')] + \mathbb{E}_{y,y'\sim q}[k(y, y')] - 2\,\mathbb{E}_{x\sim p,y\sim q}[k(x, y)].$$

C ARCHITECTURE

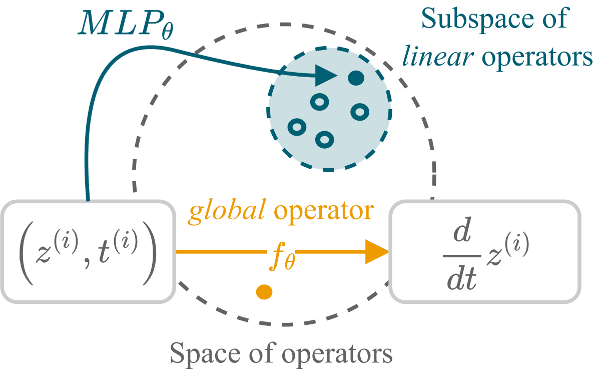

Figure 5: Visualization of the meta-learning task of Cell-MNN's encoder: Rather than directly predicting the velocity at a given operating point, as in the NeuralODE framework, the MLP of Cell-MNN maps to the space of linear operators. Conditioned on the current system state, it predicts local linear approximations to the global dynamics.

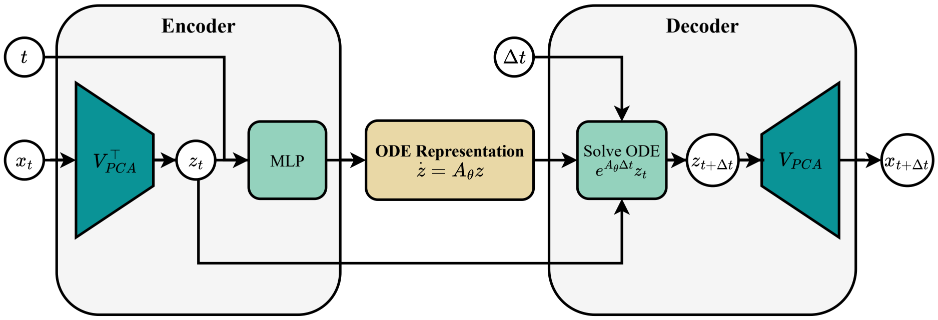

Figure 6: The Cell-MNN architecture first applies the PCA projection matrix to map the gene expression state $\boldsymbol{x}$ to a latent representation $\boldsymbol{z}_t$. An MLP then predicts a locally linear approximation $\dot{\boldsymbol{z}} = \boldsymbol{A}_\theta \boldsymbol{z}$ to the dynamics at the operating point $(\boldsymbol{z}_t, t)$. To decode, the analytical solution of this ODE is evaluated at a future time point and projected back into gene expression space.

Table 3: Collection of training hyperparameters used in all experiments. All models were trained on a single NVIDIA RTX 2080 Ti GPU. Training on EB, Cite, and Multi separately, as well as on the amortization experiment, required about 1 hour per run, while training on inflated datasets took roughly 4 hours. No distributed training or large-scale compute resources were required.

Component	**Hyperparameter**
Data preprocessing	PCA projection to 5D
MLP ($\boldsymbol{A}_\theta$)	Depth: 4
	Width: 96 (128 for amortization experiment)
	Activation: Leaky ReLU
	Initialization: Kaiming normal
	Last layer scale: 0.01
MMD kernel	Laplacian kernel $k(z, z') = \exp[-\frac{\max(\|\|z-z'\|\|_1,\epsilon)}{\sigma d_z}]$
	$\sigma = 1$, $\epsilon = 10^{-8}$
Optimization	Batch size per time point: 200
	Future discount factor $\gamma = 0.1$
	Initialization scale: 0.01
	Regularization $\lambda_{\text{kin}} = 0.1$, $\lambda_{\text{inv}} = 1$
	Optimizer: AdamW
	Learning rate: 2×10^{-4}
	Weight decay: 1×10^{-5}
Validation	Frequency: every 10 steps
	Patience: 40 validation checks
Training time	60 minutes (240 minutes for inflated datasets)
Randomness	Seeds: 3
Hardware	1× NVIDIA GeForce RTX 2080 Ti (11 GB RAM)

D PROOFS

Proposition 1 (Extension of Proposition 1 of Çimen (2010))**.** *Let* $\boldsymbol{f} : \mathbb{R}^{d_z} \times \mathbb{R} \to \mathbb{R}^{d_z}$ *satisfy* $\boldsymbol{f}(\boldsymbol{0}, t) = \boldsymbol{0}$ *for all* $t \in \mathbb{R}$*, and assume* $\boldsymbol{f} \in \mathcal{C}^k(\mathbb{R}^{d_z} \times \mathbb{R})$ *with* $k \geq 1$*. Then there exists a matrix-valued map* $\boldsymbol{A} : \mathbb{R}^{d_z} \times \mathbb{R} \to \mathbb{R}^{d_z \times d_z}$ *such that* $\boldsymbol{f}(\boldsymbol{z}, t) = \boldsymbol{A}(\boldsymbol{z}, t)\, \boldsymbol{z}$ *for all* $(\boldsymbol{z}, t) \in \mathbb{R}^{d_z} \times \mathbb{R}$*.*

Proof. Fix $(\boldsymbol{z}, t) \in \mathbb{R}^{d_z} \times \mathbb{R}$ and define $\gamma : [0, 1] \to \mathbb{R}^{d_z}$ by $\gamma(s) := \boldsymbol{f}(s \cdot \boldsymbol{z}, t)$. Since $\boldsymbol{f} \in \mathcal{C}^k$ and $k \geq 1$, the map $s \mapsto \gamma(s)$ is differentiable and

$$\frac{d}{ds}\gamma(s) = D_{\boldsymbol{z}}\boldsymbol{f}(s \cdot \boldsymbol{z}, t)\, \boldsymbol{z}.$$

By the fundamental theorem of calculus,

$$\boldsymbol{f}(\boldsymbol{z}, t) - \boldsymbol{f}(\boldsymbol{0}, t) = \gamma(1) - \gamma(0) = \int_0^1 D_{\boldsymbol{z}}\boldsymbol{f}(s \cdot \boldsymbol{z}, t)\, \boldsymbol{z}\, ds = \Big(\int_0^1 D_{\boldsymbol{z}}\boldsymbol{f}(s \cdot \boldsymbol{z}, t)\, ds\Big)\boldsymbol{z}.$$

Using $\boldsymbol{f}(\boldsymbol{0}, t) = \boldsymbol{0}$ gives $\boldsymbol{f}(\boldsymbol{z}, t) = \boldsymbol{A}(\boldsymbol{z}, t)\, \boldsymbol{z}$. □

D.1 ON THE USE OF LOW DIMENSIONAL PCA EMBEDDINGS

Low-dimensional PCA as standard practice. In line with prior work on single-cell trajectory inference, we operate in a low-dimensional latent space obtained by PCA on the gene expression matrix. Concretely, we project each dataset to the first five principal components and train both Cell-MNN and all baselines in this common representation. This choice follows the prevailing assumption in computational biology that scRNA-seq data lie near a low-dimensional manifold, and it is consistent with the implementation of *nine* previous works reported in Table 1.

Empirical validation of the 5D PCA representation. Figure 7 provides a quantitative and qualitative assessment of the 5D PCA space used in our experiments. Figures 7a, 7e and 7e show that

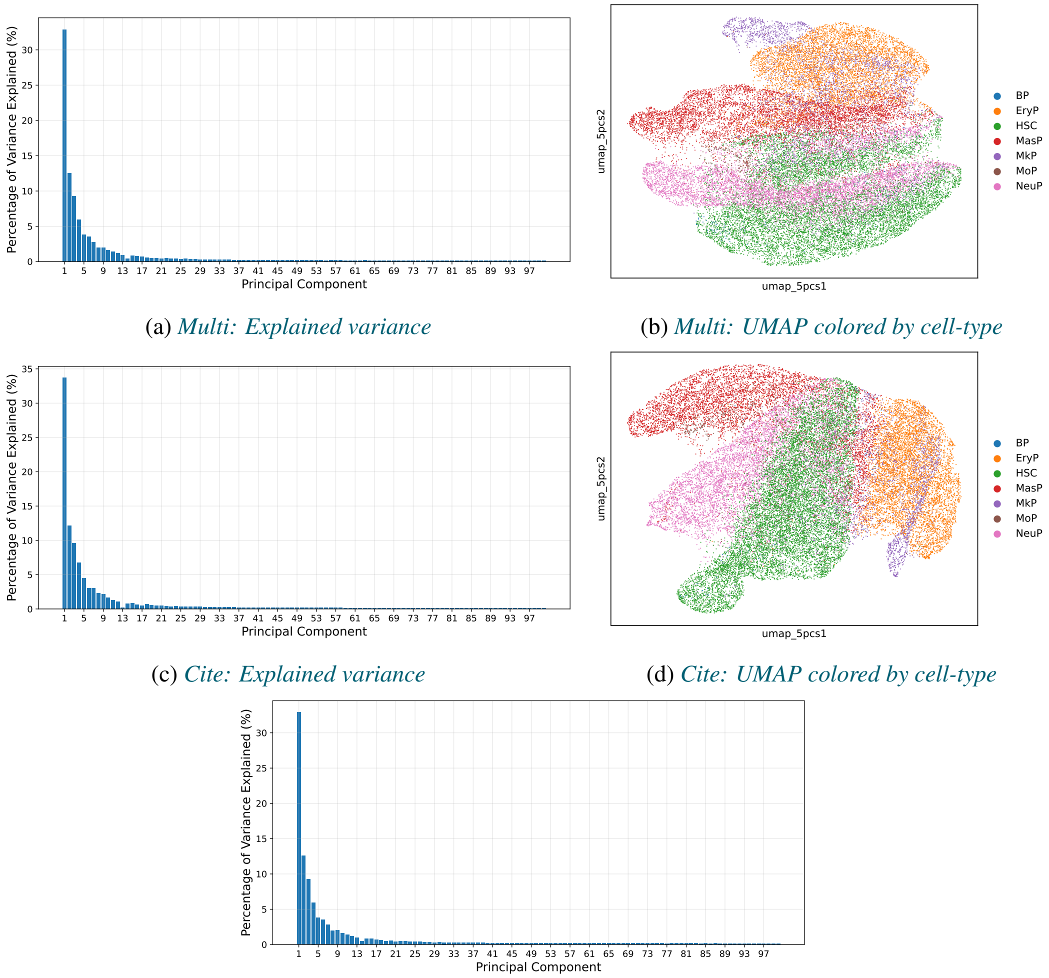

(a) *Multi: Explained variance*

(b) *Multi: UMAP colored by cell-type*

(c) *Cite: Explained variance*

(d) *Cite: UMAP colored by cell-type*

(e) *Embryoid: Explained variance*

Figure 7: (**a, c, e**) Explained variance of each of the principle components plotted for the datasets Multi, Cite and Embryoid. The first few components capture the majority of the variance. (**b, d**) UMAPs computed on the 5 dimensional PCA embedding colored by cell-type. Clustering by cell-type shows that 5 dimensional PCA embedding retains cell-type information.

the first few principal components account for the large part of the variance in each dataset: using five components yields a cumulative explained variance above 60% for Cite and Multi and above 40% for Embryoid. Importantly, this low-dimensional representation preserves cell-type structure. We compute k-nearest neighbor classification in the 5D PCA space with $k = 15$ and obtain accuracies of 87% (Multi) and 90% (Cite); for Embryoid, cell-type labels are not available. Consistently, the UMAPs computed from the 5D PCA embedding (Figures 7b and 7d) exhibit clear clustering by cell type, indicating that the embedding retains the information required to distinguish cellular lineages. To show flexibility with respect to the number of principle components used, we also train Cell-MNN and OT-CFM in 10 dimensional PCA subspace with no tuning and find that they perform similarly, see Table 10.

Scope of our contribution. Our focus in this work is orthogonal to learning the optimal representation: We focus on improving the dynamical model given a standard low-dimensional embedding. Within the 5D PCA space, Cell-MNN achieves SOTA average performance on single-cell interpolation benchmarks (Table 1), while removing OT preprocessing and learning explicit, local ODEs that can be interpreted as gene interactions. For scientific questions centered on lineage bifurcations and fate decisions, the key requirement is that the representation preserves cell-type structure. The

Table 4: Gene selection specifications for the TRRUST experiment. There are 16 genes that make up the top 10 predicted high-interaction source genes across the five time points, Of these, 14 are contained in TRRUST, and 6 have more than 10 interactions overlapping with the training gene set. This table provides shows how source genes were selected for downstream evaluation.

Top Source Gene	**In TRRUST**	**# Interactions in TRRUST**	**# in Training Gene Set**	>10 **Interactions**
HMGA1	True	18	**10**	True
HMGB2	True	2		
JUNB	True	15	4	
FOS	True	63	**25**	True
JUN	True	173	**65**	True
POU5F1	True	25	**19**	True
HAND1	False	0	0	
ID2	True	2		
TERF1	True	1		
PITX2	True	11	4	
ID3	True	2		
HMGB1	False	0	0	
SOX2	True	23	**16**	True
HMGA2	True	5		
YBX1	True	33	**24**	True
ID1	True	1		

Table 5: Validation of predicted gene interactions on TRRUST: For each source gene j, we classify each TRRUST edge $j \rightarrow i$ as activating or repressing using the sign of the learned weight $w_{j \rightarrow i}$ from Cell-MNN with one eigenvalue set to zero (averaged over cells). For each source gene, we report the number of interactions in TRRUST and classification metrics (precision, recall, and F1) shown as mean ± std across ensemble models trained on three different seeds.

Source Gene	**# Interactions** $\downarrow$	**Precision**	**Recall**	**F1**
JUN	65	$62\% \pm 8\%$	$82\% \pm 3\%$	$71\% \pm 6\%$
FOS	25	$65\% \pm 10\%$	$80\% \pm 10\%$	$71\% \pm 10\%$
YBX1	24	$55\% \pm 10\%$	$48\% \pm 3\%$	$51\% \pm 6\%$
POU5F1	19	$82\% \pm 6\%$	$58\% \pm 11\%$	$67\% \pm 6\%$
SOX2	16	$73\% \pm 12\%$	$69\% \pm 8\%$	$71\% \pm 9\%$
HMGA1	10	$78\% \pm 9\%$	$82\% \pm 2\%$	$80\% \pm 6\%$

experiments in Figure 7 show that this requirement is met. Exploring richer or alternative representations is an interesting orthogonal direction, and Cell-MNN can in principle be applied on top of such alternatives without changing the core methodology.

E Gene Regulatory Interaction Recovery

To quantitatively assess the learned gene interactions, we designed an unsupervised classification task based on the TRRUST database, which contains literature-curated gene regulatory interactions, many of which are annotated as activating or repressing. For evaluation of our model, we focus on the most dominant *source genes* predicted by Cell-MNN, i.e., those with the highest mean interaction strength with other genes. A source gene is included into the experiment if at least 10 of its interactions are listed in TRRUST. For each such gene, we classify the direction of its effect on downstream targets as activating or repressing. Since Cell-MNN produces cell-specific predictions of interaction weights, we average these over 10,000 cells to obtain a robust prediction for each interaction. Based on these predictions, we compute precision, recall, and F1 scores to quantify how well the model recovers known regulatory mechanisms and report them in Table 5 and Table 6.

Table 6: Ablation of models with *no* eigenvalue forced to zero on predicting gene interactions on TRRUST as in Table 5.

Source Gene	**# Interactions ↓**	**Precision**	**Recall**	**F1**
JUN	65	69% ± 11%	86% ± 7%	76% ± 10%
FOS	25	66% ± 22%	79% ± 19%	72% ± 21%
YBX1	24	58% ± 11%	45% ± 8%	50% ± 8%
POU5F1	19	56% ± 39%	48% ± 26%	51% ± 32%
SOX2	16	67% ± 12%	62% ± 4%	64% ± 8%
HMGA1	10	47% ± 31%	47% ± 34%	46% ± 33%

Table 7: Amortized model comparison across the *Cite* and *Multi* datasets. We report mean ± standard deviation of the EMD metric, along with the average across datasets. Lower values indicate better performance. Standard deviation is computed over left-out time points.

Model	**Cite**	**Multi**	**Average ↓**
I-CFM (Tong et al., 2024a)	0.957 ± 0.211	0.892 ± 0.092	0.925 ± 0.047
OT-CFM (Tong et al., 2024a)	0.849 ± 0.007	0.821 ± 0.013	0.835 ± 0.019
Cell-MNN	**0.795 ± 0.022**	**0.741 ± 0.104**	**0.768 ± 0.038**

Table 8: Cell-MNN ablation study on single-cell interpolation benchmark when setting one eigenvalue (EV) of $\boldsymbol{A}_\theta$ to zero. Average predictive performance degrades by less than 1%.

Method	**Cite**	**EB**	**Multi**	**Average ↓**
Cell-MNN (One EV= 0)	0.795 ± 0.016	0.701 ± 0.076	0.746 ± 0.097	0.748 ± 0.049
Cell-MNN (All EVs predicted)	**0.791 ± 0.022**	**0.690 ± 0.073**	**0.742 ± 0.100**	**0.741 ± 0.050**

E.1 Predicting the Existence of Interactions

Table 9: Comparison of GRN discovery methods on the EB dataset. We report precision@500 and AUROC for predicting existence of TRRUST interactions. Higher is better. All metrics were computed over three seeds.

Method	**Enrichment@500**	**AUROC**
GRNBoost2	20.429	0.633
SCODE	16.714	0.686
OT-CFM (J)	20.429	0,661
Cell-MNN (ours)	18.572	0.659

As an additional validation of the gene interactions predicted by Cell-MNN, we evaluate its performance at predicting the existence of regulatory links. To this end, we first rank all predicted interactions by their inferred strength and then assess this ranking against the TRRUST database. To restrict TRRUST to interactions that are plausibly involved in the differentiation dynamics of the EB dataset, we subset the database to interactions whose transcription factor (TF) regulator is mentioned as relevant in the original analysis of Moon et al. (2019) (Fig. 6d). This yields 447 interactions regulated by 70 TFs, which we treat as our ground-truth signal. This restriction is also necessary to keep the evaluation of the baselines computationally tractable. We define the candidate interaction set as all directed TF-target pairs where the TF is among the 70 EB regulators and the target is any gene in the EB dataset.

Baselines. As this experiment only requires a ranking of interactions, we can compare against methods that predict *unsigned* GRNs. We therefore include the widely used GRN discovery methods GRNBoost2 and SCODE as baselines. We also compute the performance of OT-CFM (J) on this task. Because we are only interested in the presence of a regulatory link, we evaluate all methods on the absolute interaction strength, ignoring the sign of the effect.

Evaluation and Metrics. For each method, we obtain a scalar interaction score for every TF-target pair in the candidate set, and assemble these into a TF-target score matrix in the common gene space. For Cell-MNN, interaction scores are derived from an average over 100 operators from each time point in the dataset. We use an ensemble of three Cell-MNN models each trained with a different left-out time point. For GRNBoost2 and SCODE we use their reported importance scores. We evaluate all methods using AUROC and Precision@K. The AUROC measures how well a method separates interacting from non-interacting pairs across all possible thresholds, whereas Precision@K measures the proportion of true interactions among the top-K ranked edges. To make Precision@K more interpretable, we normalize it by the base precision of a uniform ranking over all candidate interactions and refer to the resulting quantity as Enrichment@K. Intuitively, Enrichment@K measures by which factor a method outperforms random guessing.

Results and Discussion. The results of this experiment are summarized in Table 9. We find that Cell-MNN performs competitively with the baselines in terms of both AUROC and Enrichment@K. We note that we restrict GRNBoost2 to learning interactions only for the 70 EB regulators, which effectively provides them with additional prior knowledge. For both Cell-MNN and OT-CFM, we also substantially coarse-grain their outputs by averaging interaction scores across cells and discarding sign information. Consequently, both methods, which in principle can produce context-dependent, signed predictions, are evaluated here in a much more restricted, global setting.

F Additional Interpolation Results

Table 10: Model comparison on a 10-dimensional PCA embedding. We report the mean ± standard deviation of the EMD metric across the *Cite*, *EB*, and *Multi* datasets, along with the average across datasets. Lower values indicate better performance.

Method	Cite (10D)	EB (10D)	Multi (10D)	Average (10D)
OT-CFM	1.491 ±0.013	1.607 ±0.074	1.678 ±0.248	1.592 ±0.112
Cell-MNN (ours)	1.502 ±0.012	1.587 ±0.113	1.709 ±0.177	1.599 ±0.101

We provide further numerical results complementing the main experiments. For the single-cell interpolation task (Section 4.1), Table 8 reports an ablation in which the model is trained with one eigenvalue set to zero, as later used in the gene interaction discovery experiment. Table 7 presents the results of the amortization experiment across datasets (Section 4.2).

F.1 High Dimensional Experiments

In this section, we evaluate the performance of Cell-MNN in higher-dimensional latent spaces. To this end, we train the same model, with slightly modified hyperparameters, in 50- and 100-dimensional PCA subspaces. Following Neklyudov et al. (2024), we do not whiten the data in PCA space to preserve the empirical variance structure. To keep feature magnitudes in a numerically well-conditioned range for MLP training while preserving their relative variance, we rescale all components by the standard deviation of the first principal component. We find that this improves the stability of training Cell-MNN. Since the EMD is homogeneous under a global rescaling of both distributions ($\mathrm{EMD}(\lambda \boldsymbol{X}, \lambda \boldsymbol{Y}) = \lambda\ \mathrm{EMD}(\boldsymbol{X}, \boldsymbol{Y}),\ \lambda > 0$), we multiply the EMD scores computed on the rescaled PCA coordinates by the standard deviation of the first principal component so that they are comparable to those obtained on the original (unscaled) PCA space.

Due to increased RAM requirements, we use a different GPU, namely an NVIDIA L40S (48 GB RAM). This also allows us to train with a larger batch size of 1028. We set the learning rate to 1×10^{-3} (50D) and 5×10^{-5} (100D), patience for early stopping to 10 evaluation steps and keep the remaining hyperparameters unchanged. We train on the Cite and Multi and find that the runtimes range from 4m 25s to 31m 29s, depending on the seed and left-out time point. Memory usage remains below 25 GB of RAM in this setup.

We report the results of the experiments in Table 11. Without tuning the hyperparameters further, we find that Cell-MNN performs within error bars of SOTA approaches for the Multi dataset.

We remark that, due to the analytical solution of the ODE, one can choose to decode the trajectories at fewer time discretization points without impacting the accuracy of the predicted trajectories. This

Table 11: Single-cell interpolation on 50- and 100-dimensional PCA embeddings across the *Cite* and *Multi* datasets. We report the mean ± standard deviation of the EMD metric computed over three seeds. Values marked * are computed by us.

Method	**Cite** (50D)	**Multi** (50D)	**Cite** (100D)	**Multi** (100D)
I-CFM	41.834 ±3.284	49.779 ±4.430	48.276 ±3.281	57.262 ±3.855
WLF-SB	39.695 ±1.935	47.828 ±6.382	46.131 ±0.083	55.065 ±5.499
WLF-OT	38.352 ±0.203	47.890 ±6.492	44.821 ±0.126	55.416 ±6.097
OT-CFM	38.756 ±0.398	47.576 ±6.622	45.393 ±0.416	54.814 ±5.860
[SF]^{2}M-Exact	40.009 ±0.783	45.337 ±2.833	46.530 ±0.426	52.888 ±1.986
[SF]^{2}M-Geo	38.524 ±0.293	44.795 ±1.911	44.498 ±0.416	52.203 ±1.957
WLF-UOT	37.007 ±1.200	46.286 ±5.841	43.731 ±1.375	54.222 ±5.827
Cell-MNN (ours)*	38.803 ±0.635	43.926 ±2.590	46.020 ±1.177	52.698 ±2.341
OT-CFM*	38.576 ±0.429	43.141 ±3.918	45.368 ±0.473	51.399 ±3.972
OT-MFM	36.394 ±1.886	45.160 ±4.960	41.784 ±1.020	50.906 ±4.627

can be used to reduce the RAM requirements of the method and is unique when compared to Neural ODEs, whose accuracy depends on the step size due to numerical solving.

G Additional Qualitative Results

In Figures 8, 9, 10, 11, we present UMAP projections of the learned operators for each time range, colored by all the cell types reported in the developmental graph of Moon et al. (2019). These correspond to the same UMAPs described in Section 2.1, recolored by different cell type to highlight the cell-type dependence of the predicted dynamics. Cells are assigned to a type when the joint expression of the associated marker genes exceeds the 95th percentile. This analysis is enabled by having access to an explicit dynamics model conditioned on time and gene expression, which potentially allows inferences such as identifying when two cell types share similar dynamical laws within a given time range.

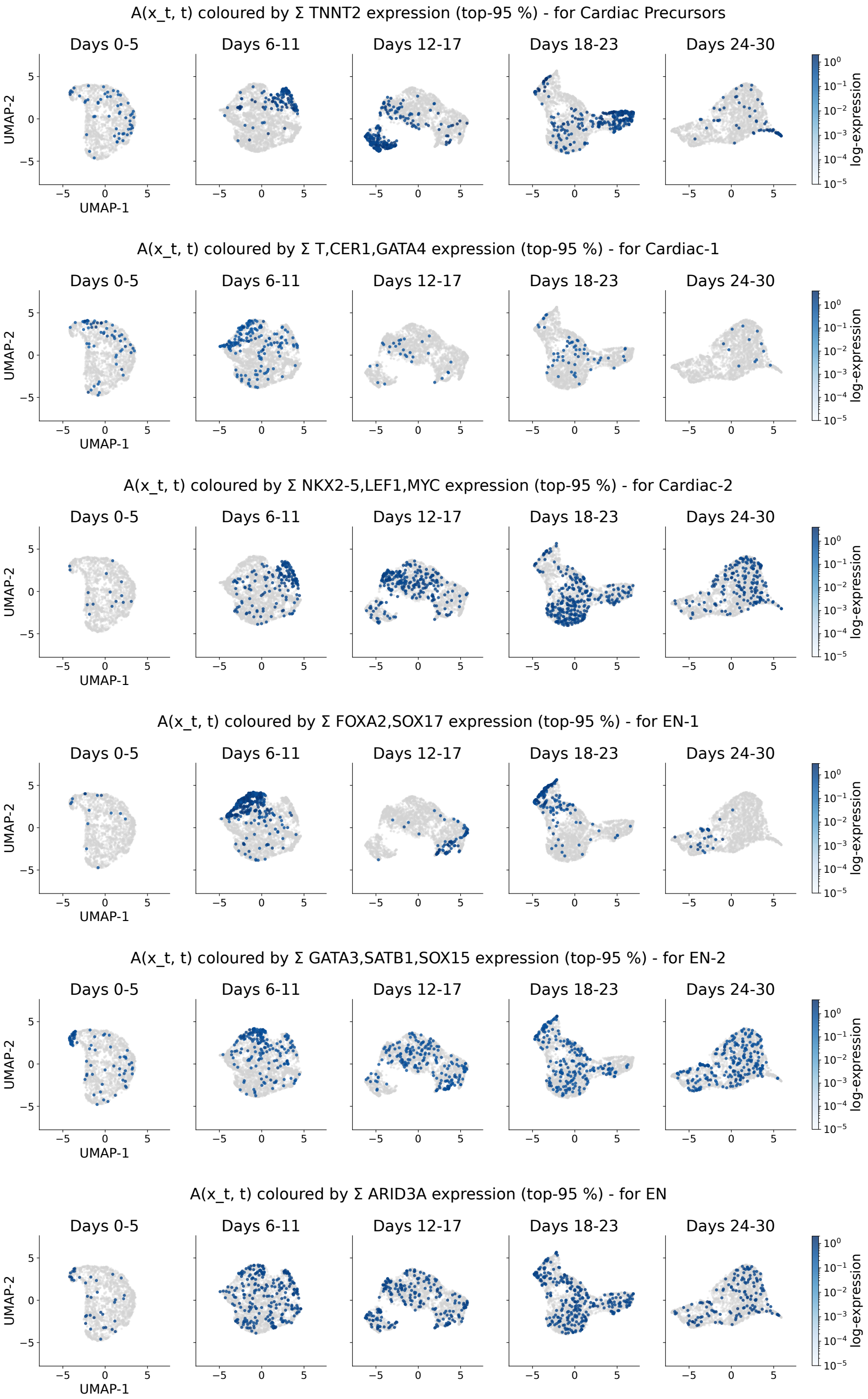
A(x_t, t) coloured by Σ TNNT2 expression (top-95 %) - for Cardiac Precursors
A(x_t, t) coloured by Σ T,CER1,GATA4 expression (top-95 %) - for Cardiac-1
A(x_t, t) coloured by Σ NKX2-5,LEF1,MYC expression (top-95 %) - for Cardiac-2
A(x_t, t) coloured by Σ FOXA2,SOX17 expression (top-95 %) - for EN-1
A(x_t, t) coloured by Σ GATA3,SATB1,SOX15 expression (top-95 %) - for EN-2
A(x_t, t) coloured by Σ ARID3A expression (top-95 %) - for EN
Days 0-5
Days 6-11
Days 12-17
Days 18-23
Days 24-30
UMAP-1
UMAP-2
−5
0
5
log-expression
10^0
10^{-1}
10^{-2}
10^{-3}
10^{-4}
10^{-5}

Figure 8

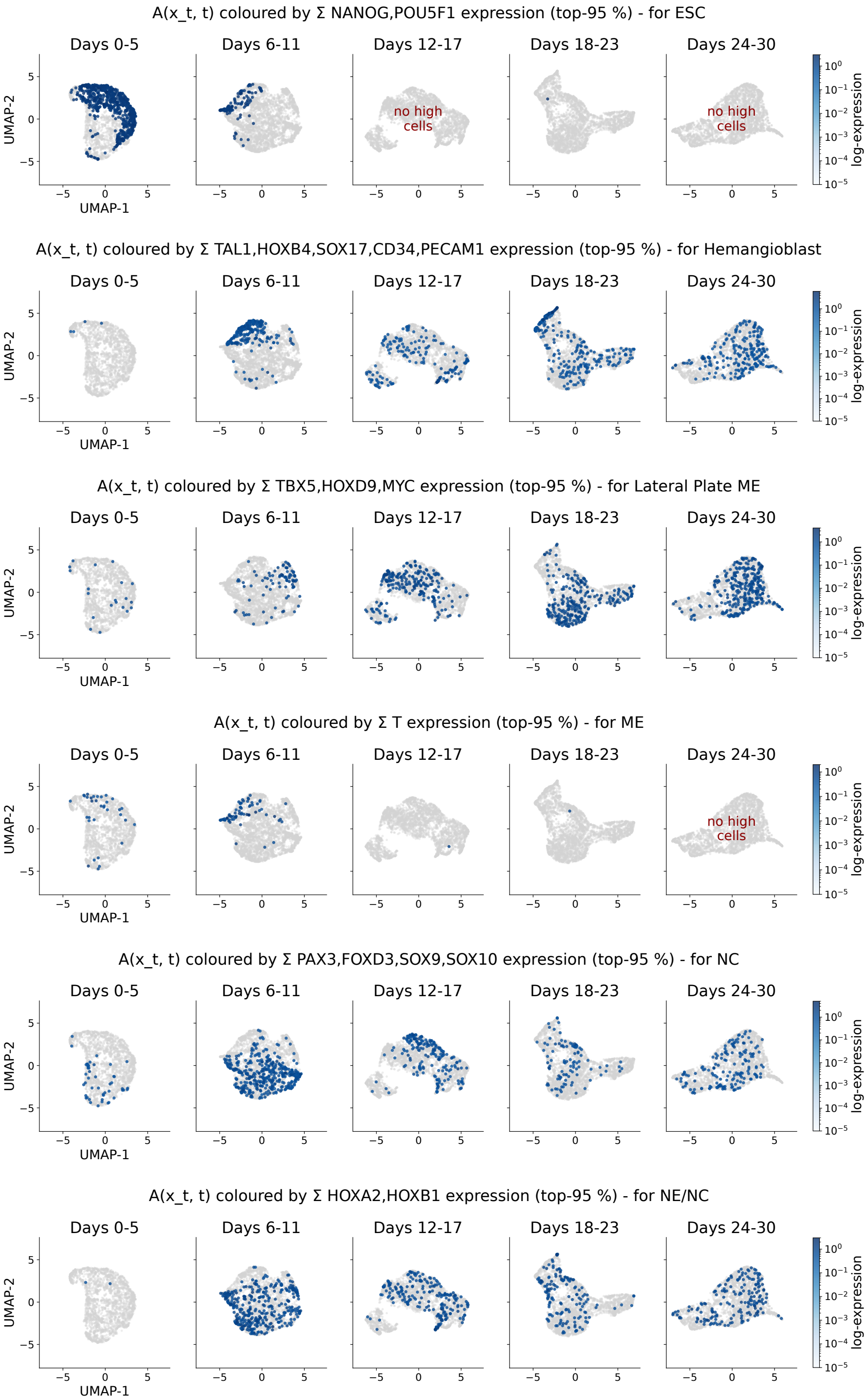

A(x_t, t) coloured by Σ NANOG,POU5F1 expression (top-95 %) - for ESC

A(x_t, t) coloured by Σ TAL1,HOXB4,SOX17,CD34,PECAM1 expression (top-95 %) - for Hemangioblast

A(x_t, t) coloured by Σ TBX5,HOXD9,MYC expression (top-95 %) - for Lateral Plate ME

A(x_t, t) coloured by Σ T expression (top-95 %) - for ME

A(x_t, t) coloured by Σ PAX3,FOXD3,SOX9,SOX10 expression (top-95 %) - for NC

A(x_t, t) coloured by Σ HOXA2,HOXB1 expression (top-95 %) - for NE/NC

Figure 9

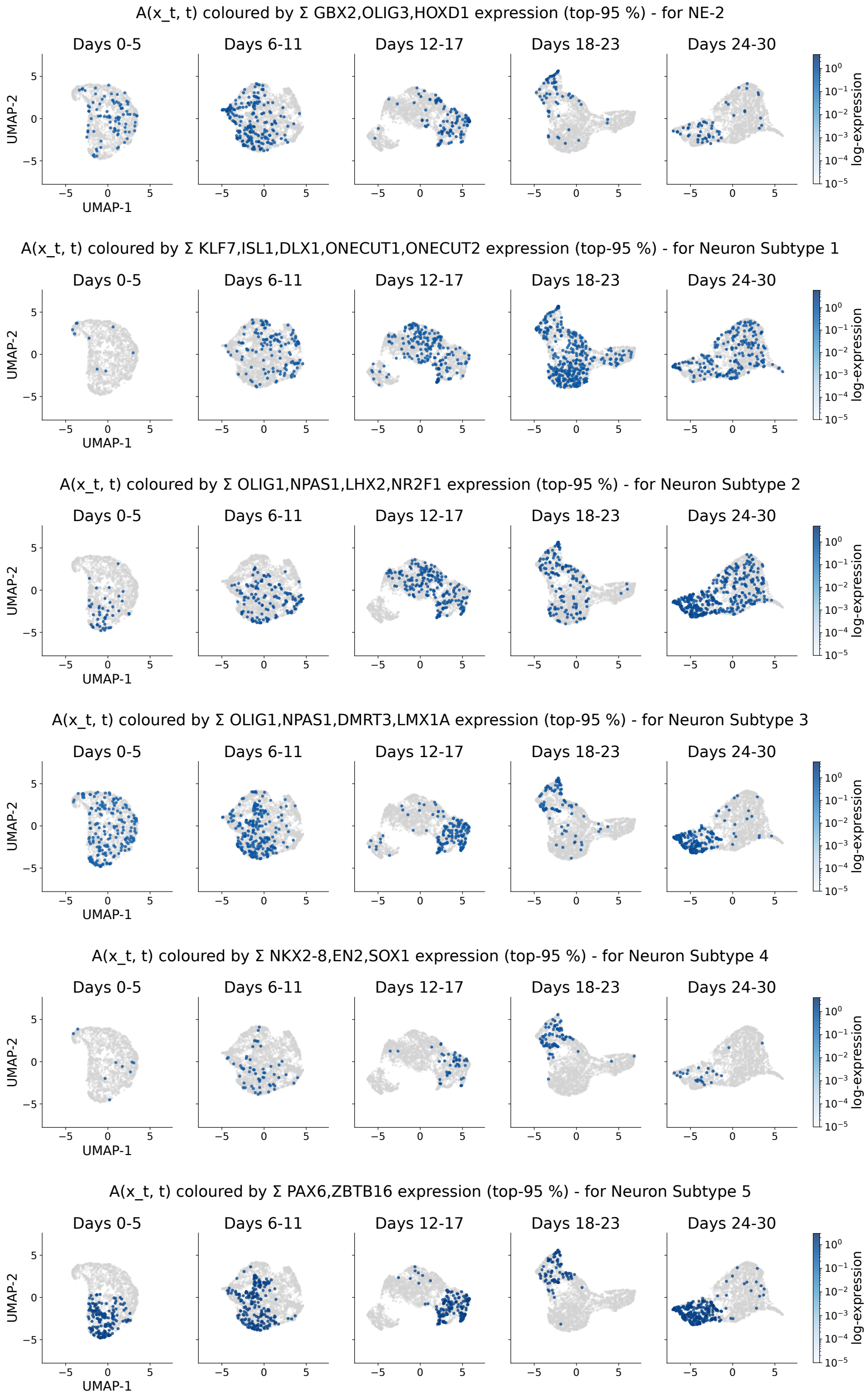
A(x_t, t) coloured by Σ GBX2,OLIG3,HOXD1 expression (top-95 %) - for NE-2
A(x_t, t) coloured by Σ KLF7,ISL1,DLX1,ONECUT1,ONECUT2 expression (top-95 %) - for Neuron Subtype 1
A(x_t, t) coloured by Σ OLIG1,NPAS1,LHX2,NR2F1 expression (top-95 %) - for Neuron Subtype 2
A(x_t, t) coloured by Σ OLIG1,NPAS1,DMRT3,LMX1A expression (top-95 %) - for Neuron Subtype 3
A(x_t, t) coloured by Σ NKX2-8,EN2,SOX1 expression (top-95 %) - for Neuron Subtype 4
A(x_t, t) coloured by Σ PAX6,ZBTB16 expression (top-95 %) - for Neuron Subtype 5
Days 0-5
Days 6-11
Days 12-17
Days 18-23
Days 24-30
UMAP-1
UMAP-2
−5
0
5
log-expression
10^0
10^{-1}
10^{-2}
10^{-3}
10^{-4}
10^{-5}

Figure 10

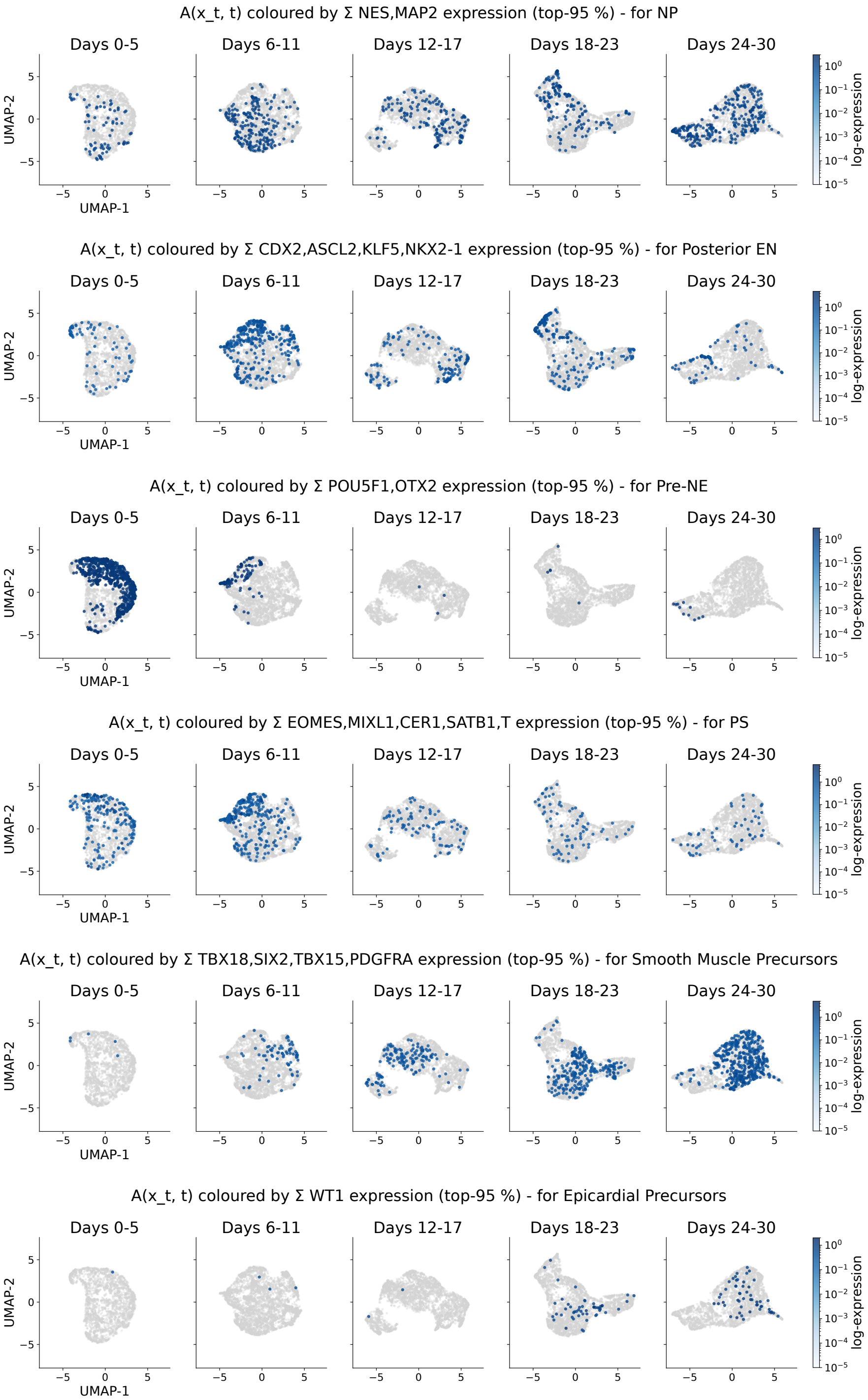

A(x_t, t) coloured by Σ NES,MAP2 expression (top-95 %) - for NP

A(x_t, t) coloured by Σ CDX2,ASCL2,KLF5,NKX2-1 expression (top-95 %) - for Posterior EN

A(x_t, t) coloured by Σ POU5F1,OTX2 expression (top-95 %) - for Pre-NE

A(x_t, t) coloured by Σ EOMES,MIXL1,CER1,SATB1,T expression (top-95 %) - for PS

A(x_t, t) coloured by Σ TBX18,SIX2,TBX15,PDGFRA expression (top-95 %) - for Smooth Muscle Precursors

A(x_t, t) coloured by Σ WT1 expression (top-95 %) - for Epicardial Precursors

Figure 11